scientific reports

Check for updates

OPEN

# Statistical-based optimization and mechanism assessments of Arsenic (III) adsorption by ZnO-Halloysite nanocomposite

Mohammad Ali Khoddam[1], Reza Norouzbeigi[1]✉, Elmira Velayi[2] & Giuseppe Cavallaro[3]

**Arsenic contamination in aqueous media is a serious environmental problem, especially in developing countries. In this research, the Box-Behnken response surface methodology was used to optimize the most relevant variables affecting arsenic adsorption on the ZnO-halloysite surface, including temperature, adsorbent dosage, pH, contact time, and As (III) initial concentration. The regression analysis indicated that the experimental data were appropriately fitted to a quadratic model with the adjusted R-squared value ($R^2$) of 0.982 for As(III) adsorption capacity and a linear model with $R^2$ of 0.931 for As(III) removal. The p-values for both adsorption capacity and removal efficiency were below 0.05, with F-values of 116.91 and 115.58, respectively, supporting the model's validity. The optimum conditions for maximum removal of As(III) were determined through numerical and graphical optimization using the desirability function. It was found that the optimum conditions for adsorption were pH = 7.99, contact time of 3.99 h, As(III) initial concentration of 49.96 mg/L, and adsorbent dosage of 0.135 g/40 ml. The accuracy of the optimization procedure was confirmed by a confirmatory experiment, which showed a maximum arsenic removal of 91.31% and an adsorption capacity of 12.63 mg/g under optimized conditions. Moreover, XPS analysis was performed at different pH levels to investigate the As (III) adsorption mechanism. The results demonstrated that As(III) adsorption occurs at acidic and neutral pH levels. On the other hand, when pH is increased to 8, As (III) oxidizes to As (V), and then adsorption occurs.**

**Keywords** ZnO-Halloysite surface, Box-Behnken design, Arsenic (III) removal, Adsorption mechanism, X-ray photoelectron spectroscopy (XPS) analysis, Numerical model

Arsenic is widely distributed in groundwater despite its relative scarcity in the natural world, and most of their types are As (III) and As(V), with contrasting toxicity levels. As (III) has 60 times more toxicity than As(V). There are several causes, including mineral dissolution, geochemical reactions, and metal ores and wood preservatives that leach arsenic compounds[1–3]. The development of biocompatible and cost-effective technologies for removing arsenic is crucial. Different technologies such as adsorption, electrocoagulation, precipitation, filtration, reverse osmosis, ion exchange, membrane, and biological methods have been used to remove arsenic-contaminated water[4–7]. Surface adsorption was the most common method since it was simple, energy-efficient, and yielded few byproducts[8]. The low cost and worldwide availability of clays make them a valuable material for contaminant adsorption. Clays are at least 20 times cheaper than activated carbon, and they are widely available worldwide. The halloysite nanotube (Hal) as clay nanomaterial could be used as an economical and biocompatible adsorbent with particularity like different electrical charges in outer and lumen surfaces[9–11]. Arsenic oxyanions (arsenites As (III)) are the major arsenic species in groundwater in pH ranges of 2 to 9 [12,13]. The lower $pH_{PZC}$ of halloysite, which is around 2.75 to 4.8 [14–16], makes it less effective at adsorbing As (III) since it exhibits cation-active behavior above pH 5 [17]. It is possible to significantly improve the sorption affinity of halloysite to oxyanions, including arsenites and arsenates, by modifying it with metals or metal oxides[13,18]. The use of nanocomposites for the treatment of dyes, inorganic compounds, and heavy metals from water and wastewater has been extensively

[1]Nanomaterials and surface technology research Laboratory, School of Chemical, Petroleum and Gas Engineering, Iran University of Science and Technology, P.B. 16765–163, Narmak, Tehran, Iran. [2]Department of Chemical Engineering, Faculty of Engineering, Azarbaijan Shahid Madani University, P.O.Box: 537517–1379, Tabriz, Iran. [3]Dipartimento di Fisica e Chimica, Università degli Studi di Palermo, Viale delle Scienze, pad. 17, Palermo 90128, Italy. ✉email: norouzbeigi@iust.ac.ir

investigated[19,20]. The Halloysite nanocomposites were typically used in the water treatment to remove organic and inorganic contaminants. Zinc oxide has antimicrobial properties, therefore it is considered one of the most important composite components in most research[21]. ZnO-Halloysite nanocomposite has been used as an economical, biocompatible, and low-toxic adsorbent for the removal of arsenic (As(III))[22,23]. Several factors affect arsenic adsorption capacity, such as temperature, solution pH, adsorbent dosage, and initial arsenic concentration[24,25]. In order to optimize adsorption processes, it is necessary to establish a logical relationship between these factors and their complex interactions. Response surface methodology (RSM) is the most potent experiment design that combines mathematical and statistical techniques for optimizing processes. One of the most reliable RSM methods is the Box–Behnken statistical experiment design method (BBD)[26–30]. By using this approach, a higher-order response surface is created than with a factorial approach, which is specially designed to fit second-order models. As a result, BBD can reveal the main effects of independent factors, the interaction effects, and the quadratic effects on the response variable[25,31–33].

Inorganic forms of As (As(III) and As(V)) are dependent on the environment's pH and redox potential. In pH less than 6, As(V) exists as $H_3AsO_4$ and $H_2AsO_4^-$, whereas in pH greater than 7, As(V) exists as $HAsO_4^{-2}$ and $AsO_4^{-3}$.The predominant species of As(III) in pH less than 7 is $H_3AsO_3$ as an uncharged molecule and in pH greater than seven as $H_3AsO_3$ and $H_2AsO_3^-$ [34,35]. In addition, the electrical charge of the surface is affected by pH and has a significant impact on arsenic adsorption.

Although arsenic adsorption mechanisms have been investigated on various adsorbents, no studies have been conducted on the mechanism of arsenic adsorption on ZnO-halloysite nanocomposite. In our previous study, the fabrication and optimization of synthesis conditions of the ZnO-Halloysite nanocomposite were studied in more detail. The major objective of this study is to investigate the arsenic adsorption mechanism onto the ZnO-halloysite nanocomposite, which is considered a nontoxic adsorbent. The RSM method was employed to determine the most appropriate combination for maximum arsenic removal and adsorption capacity and to examine the influence of key operating parameters on its adsorption.

In this work, X-ray photoelectron spectroscopy (XPS) was used to investigate the As (III) removal mechanism within the ZnO-Halloysite nanocomposite. Additionally, BBD experimental design was used to analyze and optimize the effects of adsorption conditions such as solution pH, adsorbent dosage, initial arsenic concentration, and temperature on ZnO-Halloysite nanocomposite surface adsorption capacity and As (III) removal efficiency.

## Materials and methods

### Chemical and material

Sodium arsenate solution ($NaAsO_2 > 98\%$) as As (III) standard stock and Halloysite purchased from Sigma Aldrich. The zinc acetate dihydrate [$Zn(O_2CCH_3)_2{\cdot}2H_2O$] was purchased from Across Company. Hexamethylenetetramine (HMTA, $C_6H_{12}N_4$), zinc nitrate hexahydrate ($Zn(NO_3)_2.6H_2O$), and ethanol ($C_2H_6O$) were purchased by Merck Company. Sodium hydroxide (NaOH, 99%) and hydrochloric acid (HCl, 37%) were supplied by GATRAN SHIMI TAJHIZ, an Iranian company.

### Preparation of ZnO-Halloysite nanocomposite

ZnO-Halloysite was prepared using the chemical bath deposition (CBD) method, as detailed in our previous work[22,36]. Firstly, ZnO seeds were formed on halloysite nanotubes by dip-coating halloysites in an aqueous zinc acetate solution and thermal decomposition at 500 °C (ZnO Seed-Halloysite). In the second step, zinc nitrate hexahydrate and HMTA were mixed with a constant molar ratio of 1:0.5. Following this, ZnO Seed-Halloysite was added to the prepared solution and heated at 90 °C for two hours. The solution was filtered and washed at least three times with deionized water. After collecting the powder, it was dried for one hour at 150 °C.

### Characterization

The chemical composition of samples was investigated by Fourier transform spectroscopy, FTIR (Bruker, vector 22, Germany), and X-ray photoelectron spectroscopy (XPS-PHI 5000 Versa Probe III). The XPS data was analyzed using Spectral Data Processor, SDP, v8.0 software [https://xpslibrary.com/spectra-data-processor-sdp/]. The arsenic concentration was evaluated by Atomic Adsorption Spectrometry (GBC Avanta-PM). Morphological features of the samples were evaluated by field emission scanning electron microscopy coupled with an energy dispersive spectrometer (FE-SEM, TESCAN, MIRA III) and scanning transmission electron microscopy (STEM, THERMOSCIENTIFIC, QUATTRO S SEM). The nanocomposites' Zeta potential values were measured using a Zeta potential instrument (Japan, Horiba, SZ100).

### Experimental design and statistical analysis

Design of Experiments (DOE) was used to study the effects of various factors on arsenic adsorption. It is well-known that Box-Behnken design (BBD) is one of the most useful response surface methodologies, as it utilizes both statistical and mathematical methods to optimize response. In this study, the BBD design was used to optimize the adsorption process variables to maximize arsenic adsorption capacity. The optimization process comprises three steps: identifying the problem, determining the factors and levels affecting the response, designing experiments statically, and analyzing the results[37,38]. Five factors were studied in this study, including the initial As (III) concentration, solution pH, adsorbent dosage, temperature, and contact time, in batch adsorption experiments conducted in a 100 mL glass container. Table 1 displays the levels of selected variables, which are coded as − 1, 0, and 1. Box-Behnken statistical design comprised 43 experimental points, as shown in Table 2. The center point of the design was repeated three times, and all the experiments were repeated twice. A quadratic polynomial model can approximate the relationship between independent variables and responses, as shown in Eq. (1) [32,37,39].

| Variable | Unit | Coded value and limits | | |
|---|---|---|---|---|
| | | −1 | 0 | +1 |
| Initial concentration of As(III) | mg/l | 10 | 30 | 50 |
| Adsorbent dosage (ZnO-Halloysite) | g/40 ml | 0.05 | 0.1 | 0.15 |
| Temperature | °C | 15 | 25 | 35 |
| pH | – | 4 | 6 | 8 |
| Contact time | h | 1 | 2.5 | 4 |

**Table 1**. Adsorption factors, their actual and coded levels for Box-Behnken design (BBD).

$$y = b_0 + \sum_{i=1}^{n} b_i x_i + \sum_{i=1}^{n} b_{ii} x_i^2 + \sum_{i=1}^{n-1} \sum_{j=i+1}^{n} b_{ij} x_i x_j + \epsilon \quad (1)$$

where, y is the predicted response (adsorption capacity of As(III)); $b_0$, $b_i$, $b_{ii}$ and $b_{ij}$ are the coefficients derived from polynomial regression. Additionally, $x_i$ and $x_j$ are independent variables. Lastly, ε represents the random error. Model validation was evaluated using analysis of variance (ANOVA) and lack of fit. In addition to determining the suitability and significance of a model, ANOVA can also confirm its compatibility. All the points are 3 times is repeated and average of all data is indicated. The data was analyzed using Design Expert software 13.05.0 [https://www.statease.com/trial/].

### Arsenic adsorption test

Batch adsorption experiments were performed according to our previous work[22]. Various amounts of adsorbent were in contact with As (III) solution and the solution was placed on a shaker. The shaker was operated at various temperatures (15–35 °C) at 120 rpm. The adsorbents were separated from the solution using filter paper after exposing them to As (III) for a determined period of time (1–4 h). As(III) residual concentration in the solution was measured using an atomic adsorption spectrometer. The equilibrium adsorption capacity and removal efficiency were determined by the following equations:

$$q_e = \frac{(C_0 - C_e) \times V}{m} \quad (2)$$

$$Removal\% = \frac{(C_0 - C_e)}{C_0} \times 100 \quad (3)$$

$C_o$ and $C_e$ are initial and equilibrium concentrations of As(III) (mg/L), respectively. V is solution volume (L), m is the adsorbent mass (g) and $q_e$ is equilibrium adsorption capacity (mg/g).

## Result and discussions

### Optimization of the as (III) removal using BBD

The BBD approach was applied to determine the optimum conditions for As(III) adsorption on ZnO-Halloysite nanocomposite surface. The As(III) adsorption capacity and removal efficiency as target responses (Table 2) depend on the individual or combination of selected variables. The empirical relationship between As(III) adsorption capacity and selected variables is shown in Eq. (4). Moreover, Eq. (5) provides a model for the removal efficiency of As(III). Accordingly, the experimental data on adsorption capacity was fitted on a quadratic model, while the data on arsenic removal was fitted on a linear model.

$$\begin{aligned} y = & 8.25 + 5.54A - 4.08B + 1.09\ C + 0.96D - \ 0.07E - 2.57AB + 0.58AC + 0.69AD - 1.10BC \\ & - 0.1750BD - 0.1BE - 0.045CD + 0.03CE - 0.26DE - 0.26A^2 + 2.30B^2 + 0.13C^2 + 0.09D^2 + 0.33E^2 \end{aligned} \quad (4)$$

$$y = 71.56 - 3.75A + 10.50B + 8C + 8.06D - 0.06875E \quad (5)$$

There is a general rule that both positive and negative signs have meaning in models. The positive sign describes the interactive effects of the variables on the model; in contrast, the negative sign before the model parameters represents the opposite impact or antagonistic effects on the model. The positive correlation coefficients indicate that both variables affect the response in a synergetic manner. Conversely, negative coefficients indicate an antagonistic influence on the response[39,40].

Verification of each model should be conducted using ANOVA results. The model with a P-value less than 0.05 and a high F-value is generally considered highly significant. It is necessary to conduct the Lack-of-Fit test to determine whether the model accurately matches the data. When the "Lack-of-Fit F-values" are not significant (> 0.05), it indicates that the model fits the data well. Therefore, the statistical significance of a response function must be checked with the F-test[41,42]. According to Tables 3, 4, the adsorption capacity and arsenic removal models are well-verified and predicted, and the experimental data are highly compatible.

The value of adjusted $R^2$ for the quadratic model in adsorption capacity is 0.982. This value agrees reasonably with the predicted $R^2$ of 0.963 because the difference is less than 0.2. In addition, the adjusted coefficient can be used to predict As(III) adsorption most accurately. Similarly, the adjusted $R^2$ for the arsenic removal model

| Run | Initial concentration (mg/l) - A | Adsorbent dosage (g/40 ml) - B | pH - C | Contact time (hour) - D | Temperature - E | Arsenic removal (%) | | | Adsorption capacity (mg/g) | | |
|---|---|---|---|---|---|---|---|---|---|---|---|
| | | | | | | Actual | Predicted | % Error | Actual | Predicted | % Error |
| 1 | 50 | 0.1 | 4 | 2.5 | 25 | 58 ± 0.9 | 59.8 | 3.10 | 11.5 ± 0.1 | 12.02 | 4.52 |
| 2 | 30 | 0.1 | 8 | 2.5 | 35 | 79 ± 0.8 | 79.55 | 0.70 | 9.48 ± 0.03 | 9.64 | 1.69 |
| 3 | 30 | 0.15 | 6 | 2.5 | 35 | 83 ± 0.5 | 82.05 | −1.14 | 6.6 ± 0. 2 | 6.64 | 0.61 |
| 4 | 50 | 0.1 | 6 | 4 | 25 | 77 ± 0.1 | 75.87 | −1.47 | 15.3 ± 0.11 | 15.35 | 0.33 |
| 5 | 50 | 0.15 | 6 | 2.5 | 25 | 75 ± 0.9 | 78.3 | 4.40 | 10 ± 0.4 | 9.21 | −7.90 |
| 6 | 30 | 0.1 | 6 | 2.5 | 25 | 67 ± 0.3 | 71.55 | 6.79 | 8.04 ± 0.09 | 8.55 | 6.34 |
| 7 | 10 | 0.15 | 6 | 2.5 | 25 | 85 ± 0.5 | 85.8 | 0.94 | 2.27 ± 0.03 | 3.27 | 44.05 |
| 8 | 10 | 0.1 | 6 | 4 | 25 | 85 ± 1 | 83.37 | −1.92 | 3.41 ± 0.06 | 2.88 | −15.54 |
| 9 | 30 | 0.05 | 8 | 2.5 | 25 | 75 ± 0.6 | 69.05 | −7.93 | 18 ± 0.5 | 16.98 | −5.67 |
| 10 | 50 | 0.1 | 8 | 2.5 | 25 | 73 ± 0.4 | 75.8 | 3.84 | 14.5 ± 0.1 | 15.36 | 5.93 |
| 11 | 30 | 0.1 | 6 | 4 | 15 | 81 ± 0.7 | 79.62 | −1.70 | 9.72 ± 0.03 | 9.52 | −2.06 |
| 12 | 30 | 0.1 | 4 | 2.5 | 35 | 63 ± 0.3 | 63.55 | 0.87 | 7.56 ± 0.01 | 7.46 | −1.32 |
| 13 | 10 | 0.1 | 4 | 2.5 | 25 | 68 ± 0.8 | 67.3 | −1.03 | 2.72 ± 0.05 | 2.11 | −22.43 |
| 14 | 30 | 0.1 | 6 | 2.5 | 25 | 68 ± 0.5 | 71.55 | 5.22 | 8.16 ± 0.03 | 8.55 | 4.78 |
| 15 | 10 | 0.1 | 8 | 2.5 | 25 | 85 ± 1 | 83.3 | −2.00 | 3.4 ± 0.11 | 3.13 | −7.94 |
| 16 | 50 | 0.1 | 6 | 2.5 | 15 | 70 ± 0.4 | 67.8 | −3.14 | 14 ± 0.3 | 13.69 | −2.21 |
| 17 | 30 | 0.1 | 8 | 4 | 25 | 86 ± 0.7 | 87.62 | 1.88 | 10.32 ± 0.08 | 10.61 | 2.81 |
| 18 | 30 | 0.1 | 4 | 2.5 | 15 | 65 ± 0.1 | 63.5 | −2.31 | 7.8 ± 0.5 | 7.46 | −4.36 |
| 19 | 30 | 0.1 | 4 | 4 | 25 | 73 ± 0.3 | 71.62 | −1.89 | 8.7 ± 0.3 | 8.43 | −3.10 |
| 20 | 30 | 0.15 | 6 | 4 | 25 | 93 ± 0.1 | 90.12 | −3.10 | 7.4 ± 0.4 | 7.61 | 2.84 |
| 21 | 30 | 0.05 | 6 | 4 | 25 | 65 ± 0.2 | 69.12 | 6.34 | 15.6 ± 0.1 | 15.76 | 1.03 |
| 22 | 30 | 0.1 | 4 | 1 | 25 | 54 ± 0.3 | 55.49 | 2.76 | 6.48 ± 0.07 | 6.5 | 0.31 |
| 23 | 30 | 0.05 | 6 | 2.5 | 35 | 63 ± 0.4 | 61.05 | −3.10 | 15 ± 0.4 | 14.8 | −1.33 |
| 24 | 30 | 0.05 | 4 | 2.5 | 25 | 52 ± 0.5 | 53.05 | 2.02 | 12.5 ± 0.1 | 12.61 | 0.88 |
| 25 | 30 | 0.15 | 8 | 2.5 | 25 | 89 ± 0.2 | 90.05 | 1.18 | 7.12 ± 0.02 | 6.64 | −6.74 |
| 26 | 50 | 0.05 | 6 | 2.5 | 25 | 58 ± 0.3 | 57.3 | −1.21 | 23 ± 0.45 | 22.5 | −2.17 |
| 27 | 30 | 0.05 | 6 | 1 | 25 | 56 ± 0.3 | 52.99 | −5.38 | 13.5 ± 0.3 | 13.83 | 2.44 |
| 28 | 30 | 0.1 | 6 | 1 | 35 | 67 ± 0.6 | 63.49 | −5.24 | 8 ± 0.5 | 7.59 | −5.13 |
| 29 | 30 | 0.15 | 6 | 2.5 | 15 | 88 ± 0.5 | 82.05 | −6.76 | 7 ± 0.1 | 6.64 | −5.14 |
| 30 | 10 | 0.1 | 6 | 1 | 25 | 63 ± 0.5 | 67.24 | 6.73 | 2.5 ± 0.1 | 2.35 | −6.00 |
| 31 | 30 | 0.1 | 8 | 1 | 25 | 69 ± 0.2 | 71.49 | 3.61 | 8.28 ± 0.04 | 8.68 | 4.83 |
| 32 | 30 | 0.15 | 4 | 2.5 | 25 | 75 ± 0.3 | 74.05 | −1.27 | 6 ± 0.5 | 6.65 | 10.83 |
| 33 | 30 | 0.1 | 8 | 2.5 | 15 | 80 ± 0.5 | 79.55 | −0.56 | 9.6 ± 0.5 | 9.46 | −1.46 |
| 34 | 50 | 0.1 | 6 | 1 | 25 | 58 ± 0.3 | 59.74 | 3.00 | 11.6 ± 0.3 | 12.03 | 3.71 |
| 35 | 30 | 0.1 | 6 | 2.5 | 25 | 71 ± 0.5 | 71.55 | 0.77 | 8.55 ± 0.08 | 8.55 | 0.00 |
| 36 | 30 | 0.1 | 6 | 4 | 35 | 75 ± 0.5 | 79.62 | 6.16 | 9 ± 0.1 | 9.52 | 5.78 |
| 37 | 30 | 0.1 | 6 | 1 | 15 | 64 ± 0.3 | 63.49 | −0.80 | 7.68 ± 0.2 | 7.59 | −1.17 |
| 38 | 10 | 0.1 | 6 | 2.5 | 15 | 75 ± 0.6 | 75.3 | 0.40 | 3 ± 0.4 | 2.62 | −12.67 |
| 39 | 30 | 0.05 | 6 | 2.5 | 15 | 63 ± 0.5 | 61.05 | −3.10 | 15 ± 0.5 | 14.8 | −1.33 |
| 40 | 50 | 0.1 | 6 | 2.5 | 35 | 70 ± 0.5 | 67.8 | −3.14 | 14 ± 0.5 | 13.69 | −2.21 |
| 41 | 30 | 0.15 | 6 | 1 | 25 | 75 ± 0.2 | 73.99 | −1.35 | 6 ± 0.6 | 5.68 | −5.33 |
| 42 | 10 | 0.05 | 6 | 2.5 | 25 | 63 ± 0.5 | 64.8 | 2.86 | 5 ± 0.2 | 6.29 | 25.80 |
| 43 | 10 | 0.1 | 6 | 2.5 | 35 | 75 ± 0.1 | 75.3 | 0.40 | 3 ± 0.5 | 2.62 | −12.67 |

**Table 2**. Box–Behnken design matrix and responses.

was 0.931, which aligns with the predicted $R^2$ value (0.919). A comparison of predicted and actual data for adsorption capacity and arsenic removal of As(III) is shown in Fig. 1 to confirm the model's validity. There should be a linear distribution of data points along the 45° line of the predicted versus actual graph. According to the results, the model can nearly approximate the original experimental data. Furthermore, adequate precision, as measured by dividing the effective signal by noise, can be achieved 47.62 and 37.49 for quadratic and linear model, respectively(> 4), indicating accurate result[43,44].

| Source | Sum of Squares | df | Mean square | F-value | *p*-value |
|---|---|---|---|---|---|
| Model | 878.10 | 20 | 43.91 | 116.91 | < 0.0001 |
| A-As(III) Concentration | 490.64 | 1 | 490.64 | 1306.51 | < 0.0001 |
| B-Ads. Dosage | 265.80 | 1 | 265.80 | 707.79 | < 0.0001 |
| C-pH | 19.01 | 1 | 19.01 | 50.62 | < 0.0001 |
| D-Contact time | 14.85 | 1 | 14.85 | 39.53 | < 0.0001 |
| E-Temperature | 0.0841 | 1 | 0.0841 | 0.2239 | 0.6407 |
| AB | 26.35 | 1 | 26.35 | 70.17 | < 0.0001 |
| AC | 1.35 | 1 | 1.35 | 3.58 | 0.0716 |
| AD | 1.94 | 1 | 1.94 | 5.17 | 0.0330 |
| AE | 0.0000 | 1 | 0.0000 | 0.0000 | 1.0000 |
| BC | 4.80 | 1 | 4.80 | 12.77 | 0.0017 |
| BD | 0.1225 | 1 | 0.1225 | 0.3262 | 0.5737 |
| BE | 0.0400 | 1 | 0.0400 | 0.1065 | 0.7472 |
| CD | 0.0081 | 1 | 0.0081 | 0.0216 | 0.8846 |
| CE | 0.0036 | 1 | 0.0036 | 0.0096 | 0.9229 |
| DE | 0.2704 | 1 | 0.2704 | 0.7200 | 0.4053 |
| $A^2$ | 0.4511 | 1 | 0.4511 | 1.20 | 0.2849 |
| $B^2$ | 33.86 | 1 | 33.86 | 90.17 | < 0.0001 |
| $C^2$ | 0.1103 | 1 | 0.1103 | 0.2937 | 0.5933 |
| $D^2$ | 0.0545 | 1 | 0.0545 | 0.1451 | 0.7069 |
| $E^2$ | 0.7309 | 1 | 0.7309 | 1.95 | 0.1769 |
| Residual | 8.26 | 22 | 0.3755 | | |
| Lack of fit | 8.12 | 20 | 0.4060 | 5.71 | 0.1594 |
| Pure error | 0.1422 | 2 | 0.0711 | | |
| Cor total | 886.37 | 42 | | | |

**Table 3**. ANOVA for the quadratic model of adsorption capacity.

| Source | Sum of squares | df | Mean square | F-value | *p*-value | |
|---|---|---|---|---|---|---|
| Model | 4060.63 | 5 | 812.13 | 115.58 | < 0.0001 | Significant |
| A-As(III) Concentration | 225.00 | 1 | 225.00 | 32.02 | < 0.0001 | |
| B-Ads. Dosage | 1764.00 | 1 | 1764.00 | 251.05 | < 0.0001 | |
| C-pH | 1024.00 | 1 | 1024.00 | 145.73 | < 0.0001 | |
| D-Contact time | 1040.06 | 1 | 1040.06 | 148.02 | < 0.0001 | |
| E-Temperature | 7.56 | 1 | 7.56 | 1.08 | 0.3063 | |
| Residual | 259.98 | 37 | 7.03 | | | |
| Lack of fit | 251.31 | 35 | 7.18 | 1.66 | 0.4475 | Not significant |
| Pure error | 8.67 | 2 | 4.33 | | | |
| Cor total | 4320.60 | 42 | | | | |

**Table 4**. ANOVA for the linear model for Arsenic removal.

*Effect of operation variables on adsorption performance of ZnO-Halloysite nanocomposite*

According to the ANOVA results for both responses, adsorption capacity and removal efficiency of As (III) presented in Tables 3, 4, the corresponding models are highly significant with P-values less than 0.01. For both models, the terms of arsenic concentration (A), adsorbent dosage (B), solution pH (C), and contact time (D) are highly significant, but temperature (E) is insignificant with a P-value greater than 0.1 [45,46]. Consequently, the insignificant model term was eliminated using the backward elimination method with an alpha value greater than 0.05 and based on the P-value as a criterion. This improved the model predictability for As (III) adsorption capacity. The lack of fit for the reduced quadratic model (Eq. (6)) was recalculated, resulting in a non-significant value of 0.2014. The ANOVA result is mentioned in Table 5. Moreover, after using the backward elimination method, adequate precision is reached to 73.77.

$$y = 8.56 + 5.54A + 4.08B + 1.09C + 0.96D - 2.57AB + 0.58AC + 0.69AD - 1.10BC - 0.40A^2 + 2.16B^2 \quad (6)$$

Moreover, significant model in linear for Arsenic removal as response after model modification by backward elimination process based on P-value as a criterion is shown in (Eq. (7)). The ANOVA result is mentioned

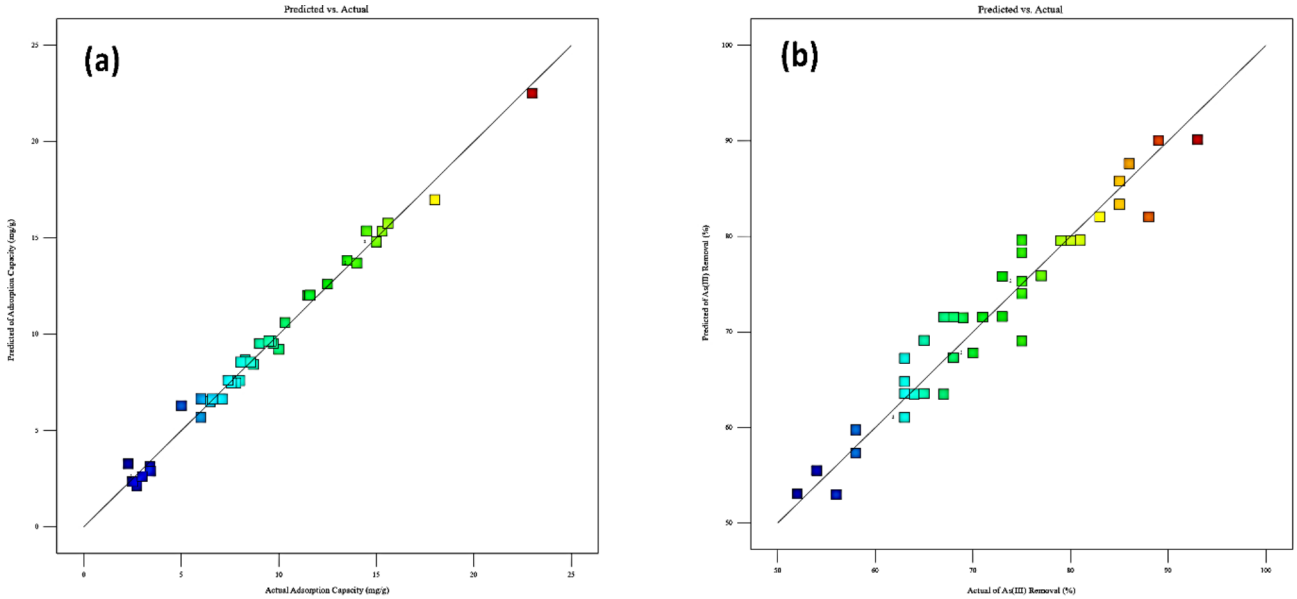


**Fig. 1**. The predicted values versus experimental or actual values of As(III) adsorption capacity (**a**) and AS(III) removal (**b**) over ZnO-Halloysite.

| Source | Sum of squares | df | Mean square | F-value | *p*-value |
|---|---|---|---|---|---|
| Model | 876.81 | 10 | 87.68 | 293.59 | < 0.0001 |
| A-As (III) Concentration | 490.64 | 1 | 490.64 | 1642.87 | < 0.0001 |
| B-Ads. Dosage | 265.80 | 1 | 265.80 | 890.01 | < 0.0001 |
| C-pH | 19.01 | 1 | 19.01 | 63.65 | < 0.0001 |
| D-Contact time | 14.85 | 1 | 14.85 | 49.71 | < 0.0001 |
| AB | 26.35 | 1 | 26.35 | 88.24 | < 0.0001 |
| AC | 1.35 | 1 | 1.35 | 4.51 | 0.0416 |
| AD | 1.94 | 1 | 1.94 | 6.51 | 0.0157 |
| BC | 4.80 | 1 | 4.80 | 16.06 | 0.0003 |
| $A^2$ | 1.55 | 1 | 1.55 | 5.21 | 0.0293 |
| $B^2$ | 45.29 | 1 | 45.29 | 151.67 | < 0.0001 |
| Residual | 9.56 | 32 | 0.2986 | | |
| Lack of fit | 9.41 | 30 | 0.3138 | 4.41 | 0.2014 |
| Pure error | 0.1422 | 2 | 0.0711 | | |
| Cor total | 886.37 | 42 | | | |

**Table 5**. ANOVA for the reduced quadratic model for adsorption capacity.

in Table 6. Moreover, after using the backward elimination method, adequate precision is reach to 41.03 and predicted $R^2$ is reach to 0.92.

$$y = 71.56 - 3.75A + 10.50B + 8C + 8.06D \quad (7)$$

*Response surface studies and contour plots*

Contour plots and 3D response surface graphs are shown in Fig. 2 to assess the influence of five variables on adsorption capacity. The graphs illustrate how two main variables affect the response at a constant level of the other variables. According to Eq. 6, which appears in Table 5, the effectiveness of the model's factors determines the consequences of interactions in 3D graphs (AB > BC > AD > AC). As stated, AB and BC have antagonistic effects on adsorption capacity since they have negative signs in the model, while AD and AC have positive signs, resulting in synergetic effects[47,48]. According to Fig. 2, following the reduced quadratic model (Eq. (6)), the effect of temperature is eliminated by the high P-value. As shown in Fig. 2b, f, the adsorption capacity increases as the As (III) concentration (A) and contact time (D) simultaneously increase. The relation between initial concentration (A) and solution pH (C) at a constant medium level of other variables is presented in Fig. 2c, g. At low As (III) initial concentrations, pH variations from acidic to alkaline lead to a slight increase in adsorption capacity. However, at higher As(III) initial concentrations, pH effects become more pronounced. Based on the

| Source | Sum of squares | df | Mean square | F-value | *p*-value | |
|---|---|---|---|---|---|---|
| Model | 4053.06 | 4 | 1013.27 | 143.92 | < 0.0001 | Significant |
| A-As(III) Concentration | 225.00 | 1 | 225.00 | 31.96 | < 0.0001 | |
| B-Ads. Dosage | 1764.00 | 1 | 1764.00 | 250.55 | < 0.0001 | |
| C-pH | 1024.00 | 1 | 1024.00 | 145.44 | < 0.0001 | |
| D-Contact time | 1040.06 | 1 | 1040.06 | 147.72 | < 0.0001 | |
| Residual | 267.54 | 38 | 7.04 | | | |
| Lack of fit | 258.88 | 36 | 7.19 | 1.66 | 0.4472 | Not significant |
| Pure error | 8.67 | 2 | 4.33 | | | |
| Cor total | 4320.60 | 42 | | | | |

**Table 6**. ANOVA for the reduced linear model for arsenic removal.

$pH_{PZC}$ value, the surface charge of As(III) species was negative above pH 7, and the predominant species of As(III) are $H_3AsO_3$ and $H_2AsO_3^-$. The increase in adsorption capacity may be due to oxidation of As(III) and conversion to As(V), as well as surface complex formation between As(V) and ZnO-Halloysite surface functional groups[22,49]. As already mentioned, As(III) initial concentration (A) and adsorbent dosage (B) have antagonistic effects on adsorption capacity, i.e., an increase in As(III) initial concentration and a decline in adsorbent dosage leads to an increase in adsorption capacity (Fig. 2a, e). A similar relationship is observed between adsorbent dosage (B) and solution pH (C) (Fig. 2d, h). By increasing the pH of the solution and reducing the adsorbent dosage, the adsorption capacity is increased.

Optimization based on the desirability function. Using numerical optimization, a desirable value for each input factor and response can be selected. For a given set of conditions, possible input optimizations include range, maximum, minimum, target, none (for response), and set to determine the optimal output value. In this study, input variables were given specific ranges of values, while As (III) removal efficiency was aimed at a maximum, and As (III) adsorption capacity was considered a target. Minimum and maximum target values were set between 5 and 25 mg/g. Figure 3 illustrates ramp function graphs with blue and red dots for five key factors and their two responses. Factors and responses are represented by red and blue dots, respectively. The height of the dot corresponds to the level of desirability upon optimization. According to Fig. 3, the values of optimal conditions for independent variables were obtained as follows: pH = 7.99, contact time of 3.9 h, As (III) initial concentration of 49.99 mg/L, and adsorbent dosage of 0.135 g/40 ml. Using these conditions, the degree of desirability of the model was 0.955, the maximum achieved removal percentage of As (III) was 91.31%, and the adsorption capacity as the target was 12.63 mg/g. The confirmatory experiment demonstrated that AS(III) removal was 89.2% and As (III) adsorption capacity was 12.1 mg/g under optimal conditions, compared to the model's removal of 91.31% and adsorption capacity of 12.63 mg/g. This indicates that the model is suitable and accurate.

Moreover, the graphical optimization as contour graphs of As (III) removal, adsorption capacity, and desirability are shown in Fig. 4. Gradient colours are used in the graph, with blue representing a low level of desirability and warm yellow representing a high level. In the contour plot, the flags show the optimal point for achieving 95.5% desirability, 91.31% As (III) removal efficiency, and 12.63 mg/g adsorption. As all the information has been summarized, the factors are considered AB.

## FTIR analysis and effect of pH

FTIR analysis was conducted to study the chemical stability of ZnO-Halloysite nanocomposites surface under various pH conditions. ZnO-Halloysite nanocomposite was exposed to acidic (pH = 2), slightly acidic and basic (pH = 4 and 8), neutral, and pH of 10 and 12 media for 24 h. Figure 5 shows the FTIR spectra of ZnO-Halloysite after exposure to different pH media. In the ZnO-Halloysite spectra, bands at 440, 470, 516, 640, and 782 $cm^{-1}$ can be attributed to Zn-O stretching vibrations. The band at 3428 cm corresponds to the stretching vibration of hydroxyl groups. There are peaks at 1106, 804, and 928 $cm^{-1}$, which correspond to asymmetric vibrations of Si-O-Si and bending vibrations of Si-OH. The bands observed at 1338 and 1341 $cm^{-1}$ are assigned to the bending and wagging vibrations of C-H groups, respectively. The band at 1635 $cm^{-1}$ is related to the asymmetric vibration of C = O. There is a peak at 1565 $cm^{-1}$ associated with the C-C stretching vibration.

Comparing ZnO-Halloysite spectra at different pH confirms that the intensity of peaks relating to the ZnO particles was reduced on ZnO-Halloysite nanocomposite (peaks 440, 473, 516, and 782 $cm^{-1}$) in highly acidic and alkaline solutions. These findings indicate the structure is inherently unstable in acidic and alkaline environments. The destruction of ZnO nanoparticles in acidic conditions is more significant than in alkaline environments. However, zinc oxide particles do not necessarily dissolve in acidic and alkaline environments due to their varying solubilities in different pH[50–53]. As a result, the nanocomposites are stable at neutral pH, but zinc ions are dissolved significantly in highly acidic (pH = 2) and highly alkaline (pH = 12) environments. Similar results have been reported by other researchers[54,55]. The other dramatic changes may result from the degradation of the silica phase in the nanocomposite (804, 914, 1106 $cm^{-1}$). Moreover, there is an absorption peak between 1710 and 1760 $cm^{-1}$[11] for the C = O bond. Table 7 summarizes the characteristics of the stretching vibration bands associated with the bonds.

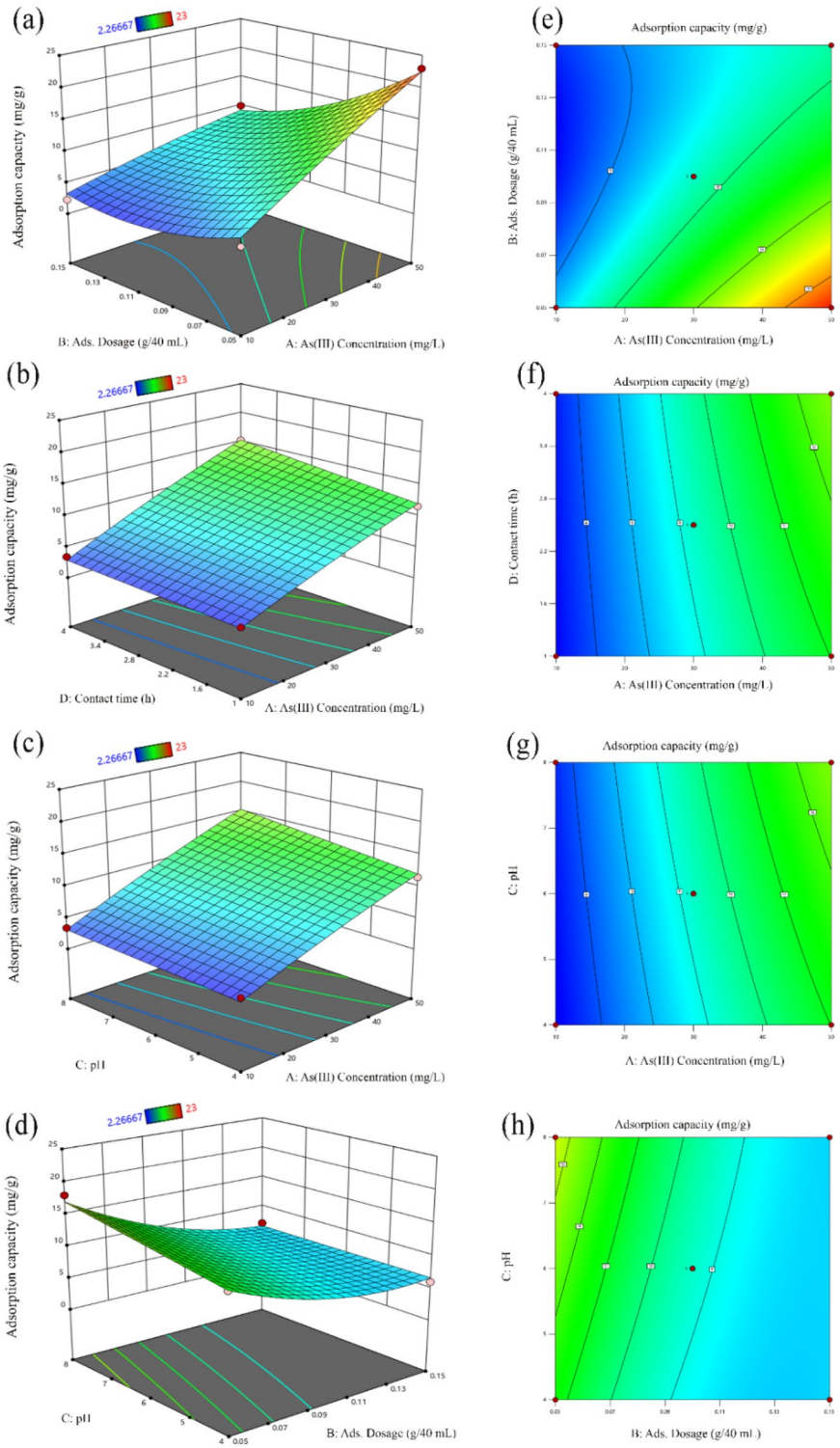


**Fig. 2**. Response surface plots (**a-d**) and contour line of interaction effects between each factor (**e-h**) on total arsenic adsorption capacity.

## XPS analysis

Figure 6 shows the XPS survey spectra of Halloysite, ZnO seed-Halloysite, and ZnO-Halloysite surfcae. According to Fig. 6, carbon, oxygen, aluminum, and silicon are present in Halloysite. Furthermore, zinc is observed in ZnO seed-Halloysite and ZnO-Halloysite on nanotube and nanocomposite surfaces. Additionally, Table 8 shows a quantitative comparison of the XPS results of the above compounds.

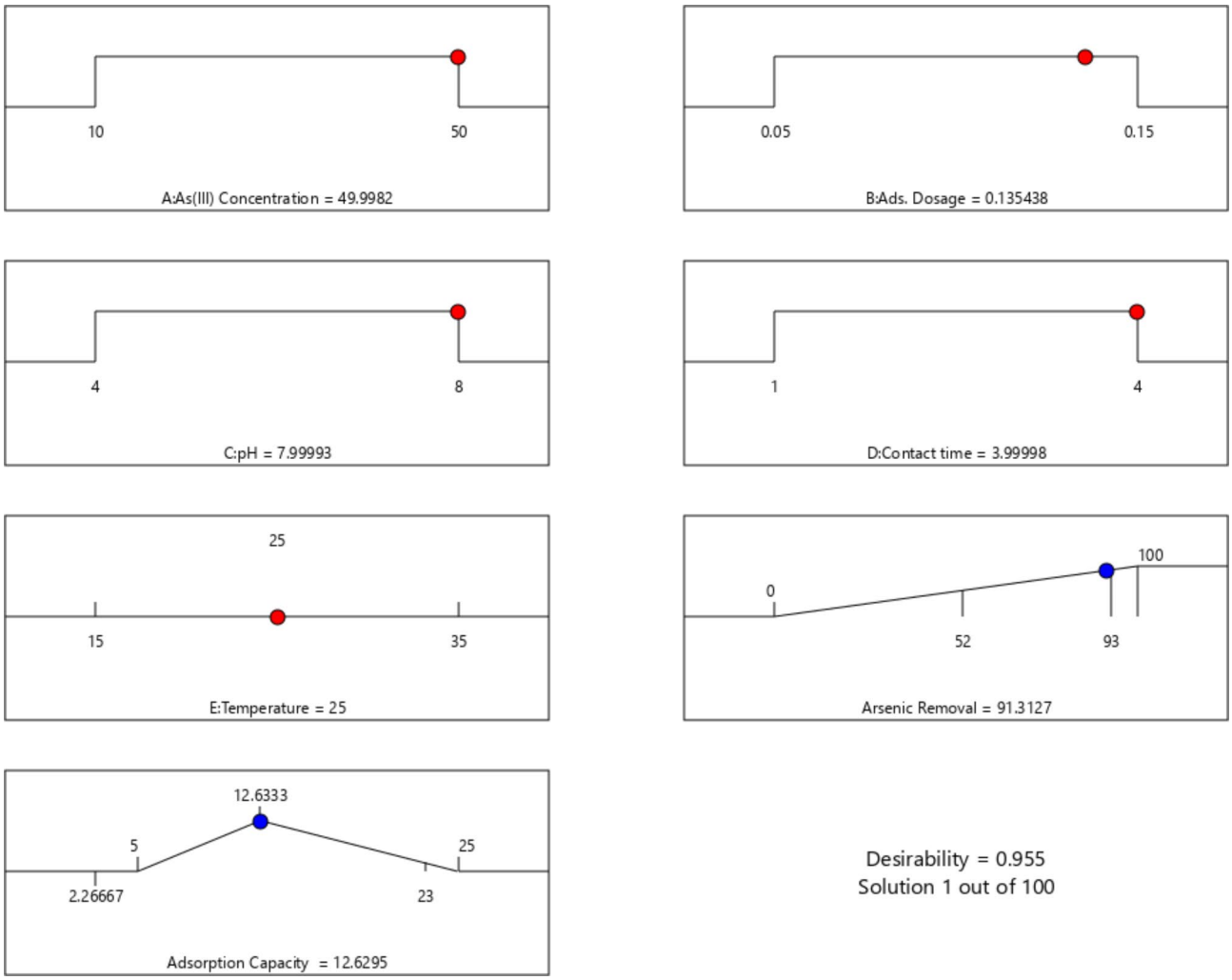


**Fig. 3**. The desirable ramp for optimizing the adsorption capacity as the target.

Table 8 summarizes the atomic ratios and contents of the samples. According to Fig. 6c, ZnO-Halloysite shows two strong peaks at 1046.1 and 1023.1 eV related to the binding energies of Zn $2p_{1/2}$ and Zn $2p_{3/2}$. It was estimated that the energy difference between the two peaks was 23 eV, similar to that of typical ZnO nanoparticles, thus providing support for the +2 valence state of Zn in ZnO[56]. Compared with ZnO seed-Halloysite and ZnO-Halloysite, ZnO particles are more abundant in ZnO-Halloysite surface. A higher amount of C1s is associated with the presence of HMTA. The O1s spectra of Halloysite and ZnO-Halloysite samples are shown in Fig. 7; the deconvoluted O1s spectra in Halloysite (Fig. 7a) showed three peaks centered 530.4, 531.6, 532.5 eV, which were assigned to surface hydroxyl groups, $Al_2O_3$ and $SiO_2$[57,58]. The deconvolution of O1s peaks was performed using the Gaussian function.

Moreover, the deconvoluted O1s spectrum for ZnO-Halloysite (Fig. 7b) shows four peaks centered in 528.8, 531.3,533 and 534.2. The band at 528.8 is attributable to the $O^{2-}$ ions bond with Zn+2 ions in the wurtzite structure of ZnO[57,59–63]. Furthermore, the bands at 531.3 might be related to OH groups derived from $OH^-$ radical adsorption or $Zn(OH)_2$ on the surface[64,65] or oxygen vacancies in ZnO[66–68]. Furthermore, binding energy centered at 531.3 is described as C=O in some literature[69,70]. The peak at a binding energy of 533 eV can be attributed to surface hydroxyl or Zn–O–Si groups in halloysite and to chemically attached oxygen species like $H_2O$ and $O_2$ on ZnO surfaces[64,71–73]. Additionally, the band at 534.2 eV could probably be attributed to O-C=O surface bonding on ZnO or $Zn_2SiO_4$ surfaces[73,74].

## Effect of pH on the as (III) adsorption

Based on our previous work, $pH_{PZC}$ for ZnO-Halloysite was reported to be nearly 6.9 as a function of zeta potential[22]. Accordingly, the surface charge of ZnO-Halloysite is negative above $pH_{pzc}$. Since As (III) species have neural or negative surface charge up to pH 8, arsenic adsorption is expected to decline above $pH_{pzc}$. However, the results, as mentioned above, showed that the adsorption capacity increased with an increase in pH from 6 to 8. In order to better understand the effect of solution pH on the adsorption of As(III) on ZnO-Halloysite composites, XPS analysis was performed. Numerous studies have reported the effectiveness of nanomaterials in removing arsenic ions from water. Reddy et al.[75], reported that CuO nanoparticles can remove As(III) and As(V) under

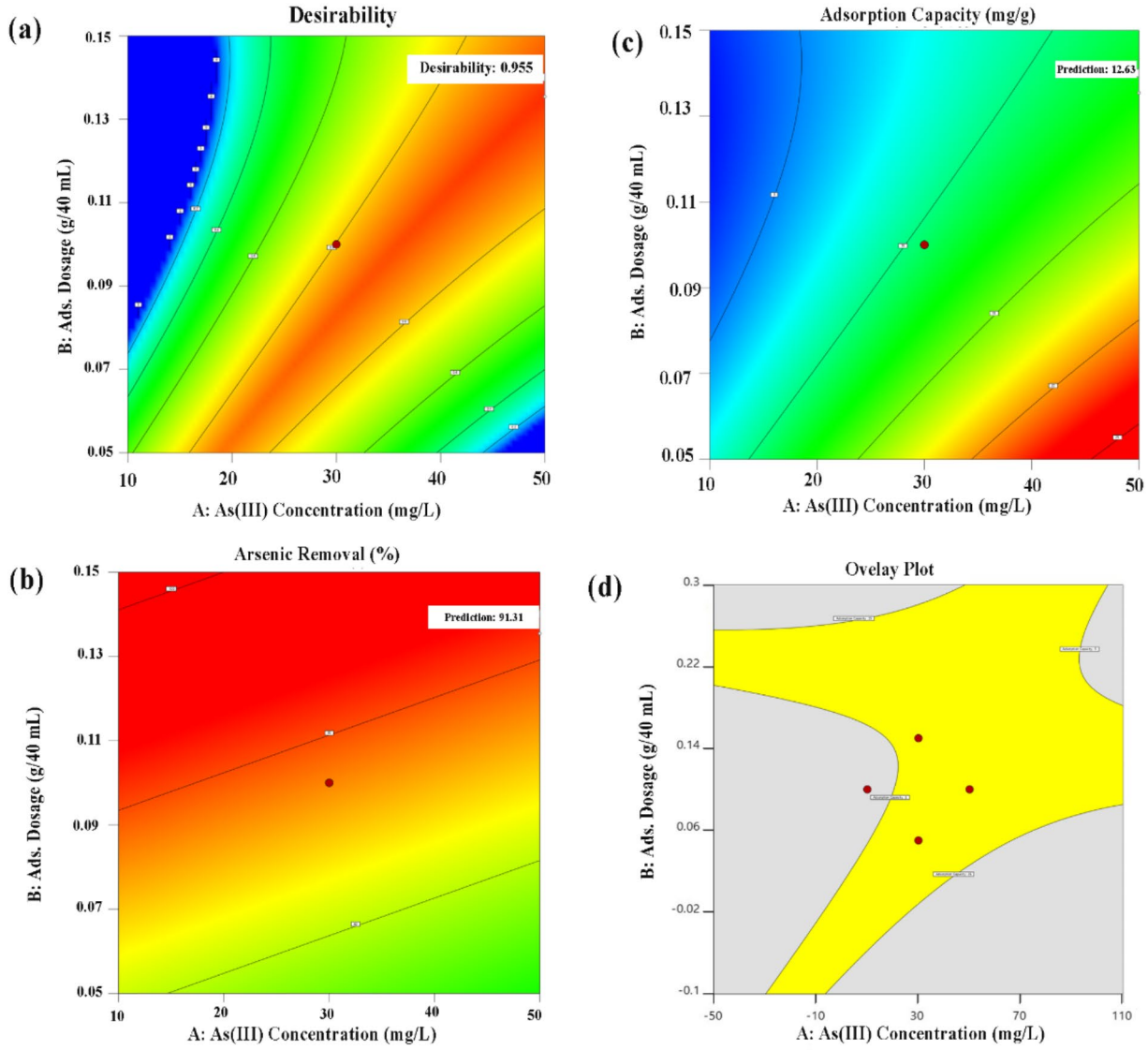


**Fig. 4**. (**a**) Contour plot for desirability achievement based on the specified criteria, contour plots for (**b**) adsorption capacity, (**c**) arsenic removal, and (**d**) overlay plot to As (III) concentration and adsorbent dosage.

a wide pH range due to the high pHpzc ($pH_{pzc}$=9.4(. Moreover, this study indicated that the As(III) adsorption rate is slower than that of As(V). Three characteristic peaks at 45.15, 45.28 and 45.2 eV were identified as As(V) in XPS analysis, which was approximately 1 eV more than the position associated with As(III)[76]. According to the research published by sofer et al., the bands at 41.5 and 42.2 eV were correlated with $As3d_{5/2}$ and $As3d_{3/2}$ while binding energies at 44.9 eV were related to As(III) as As(III) trioxide[77]. It has been reported that the binding energies of As3d in arsenic oxides are in the range of 44.3–44.5, and 45.2–45.6 eV[78]. Summary of some of the binding energies stated in the previous studies is presented in Table 9. Figure 8 illustrates high-resolution As3d XPS spectra after As (III) adsorption onto ZnO-Halloysite at different solution pH. Using Gaussian fitting analysis, the As3d spectrum of ZnO-Halloysite-As was deconvoluted into three characteristic peaks between 38 and 49 eV. The surface atomic content and ratios of arsenic species are presented in Table 10.

Based on the results, the adsorbed arsenic on ZnO-Halloysite nanocomposite surface is predominately present in As(III) at all pH levels. As (V) was also observed in the As3d spectra of all ZnO-Halloysite-As nanocomposite with atomic ratios of 27, 34.6, and 38.4% respectively as mentioned in Table 10, for pH ranges 4, 6, and 8. It can be concluded from this observation that As(III) was partially oxidized to As(V) during the adsorption reaction. The dominant species, $H_3AsO_3$ generally dissociates into $H_2AsO_3^-$, $HAsO_3^{2-}$, and $AsO_3^{3-}$[83]. pH can affect the oxidation rate of the As(III) in these three forms[49]. According to the results, As(III) oxidized faster at pH 8 compared to pH 6 or 4.

Moreover, as shown in Fig. 8d, intensity of binding energy in pH equal to 8 is more than 4 and 6, this point is confirmed the optimum operational condition which is derived from adsorption capacity model.

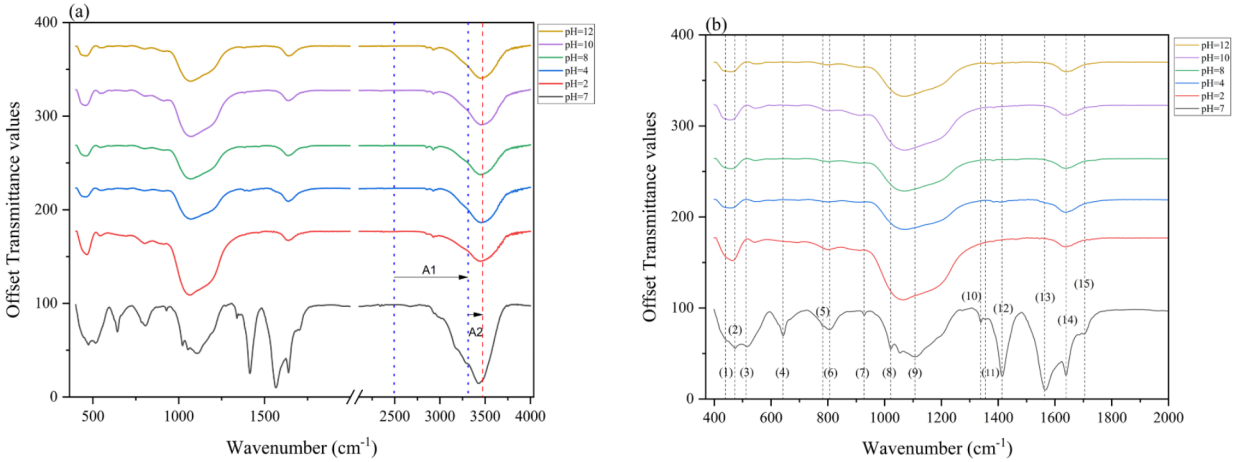


**Fig. 5**. FTIR spectra curves between (**a**) 400 $cm^{-1}$ to 4000 $cm^{-1}$ and (**b**) 400 $cm^{-1}$ to 2000 $cm^{-1}$ of ZnO-Halloysite after exposure to different pH media.

| Range or points | Wavenumber ($cm^{-1}$) | Band assignments |
|---|---|---|
| A1 | 2500–3000 | O-H bonds |
| A2 | 3300–3400 | O-H stretch |
| 15 | 1709 | C = O stretch |
| 14 | 1635 | C = O stretch |
| 13 | 1565 | C-C stretch |
| 12 | 1412 | O-H bend |
| 10, 11, 8 | 1338–1350, 1020 | C-H group |
| 9, 6, 7 | 1106, 928, 804 | Si-O-Si and bending vibrations of Si-OH |
| 1, 2, 3, 4, 5 | 440, 470, 516, 640, 782 | Zn-O stretch |

**Table 7**. Positions and assignments of the IR vibration bands.

## EDX analysis

To further investigate the chemical composition of ZnO-Halloysite surface after arsenic adsorption, the EDX analysis was performed. Figure 9 shows the EDX spectrum and elemental mapping of ZnO-Halloysite nanocomposite surface after As (III) adsorption at pH 8. The results showed that ZnO-Halloysite nanocomposite adsorbent adsorbed arsenic. The elemental mapping graphs clearly show that elemental arsenic is abundant and uniformly distributed in the adsorption products, demonstrating ZnO-Halloysite nanocomposites' excellent adsorption abilities.

## Arsenic removal mechanism

The adsorption of arsenic on ZnO-Halloysite nanocomposite includes a hard acid-hard base interaction as well as surface complexation between arsenic and ZnO-Halloysite nanocomposite. Hard acid and hard base reactions might occur in the pH range of 7 to 8 due to hydroxyl groups. According to the results, the maximum adsorption of arsenic was found in the 7.0–8.0 pH range. Arsenic (III) has a neutral form ($H_3AsO_3$) or negative surface charge in this pH range. The hydroxyl groups on the ZnO-Halloysite surface can deprotonate under these conditions and attach to arsenic (III). A similar mechanism is reported for arsenic removal by zinc peroxide functionalized synthetic graphite[84].

It is possible for As(III) and ZnO-Halloysite to form complexes due to As(III) doping caused by native defects in ZnO nanoparticles, such as O vacancies and Zn interstitials. Generally, Arsenic in ZnO may occupy the Zn site ($As_{zn}$), O site ($As_O$), or the interstitial position ($As_i$)[85]. According to some studies, As(III) does not necessarily occupy the O site; however, $As_{zn}$-$2V_{zn}$ and $As_{zn}$-$3V_{zn}$ may form[86,87].

According to the literature, binding energy of 47–48 eV is attributed to As in $As_o$ (As occupying an O site), which can serve as a deep acceptor ($As_o$). Binding energy in the range of 41 to 42 may relate to $As_{Zn}$, which acts as a donor bond. In addition, $As_{Zn}$–$2V_{Zn}$ is another possible acceptor defect related to arsenic occupying zinc sites inducing two vacancies. The $As_{Zn}$–$2V_{Zn}$ has a very similar binding energy to $As_{Zn}$. In the $As_{Zn}$– $2V_{Zn}$ complex, the As (III) atom donates all three electrons simultaneously to each of the two $V_{Zn}$ that can accept two electrons. $As^{3+}$ will sit in the geometry of a wurtzite structure in a highly electronegative environment with

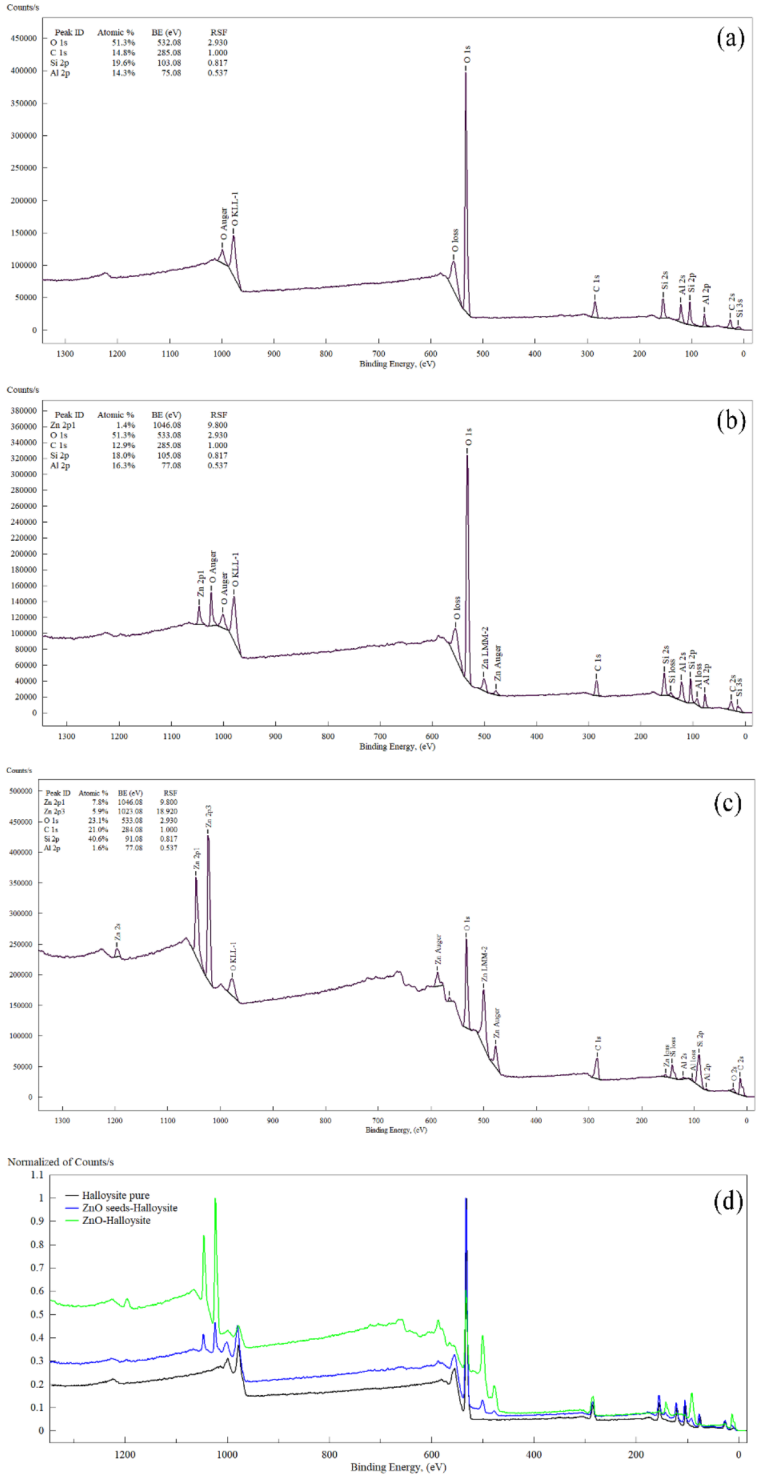


**Fig. 6**. XPS Survey spectra of Halloysite pure (**a**), ZnO Seed-Halloysite (**b**), ZnO-Halloysite (**c**), and overlay of all survey spectra (**d**).

negative oxygen ions. The band at a binding energy of 42 eV is assigned to $As_i$, which acts amphoteric. As-O and As-Zn bindings should not appear if arsenic occupies the oxygen or zinc sites[85,88–93]. According to the XPS results, the As–O bonding is not visible, but the As–Zn bonding is visible, showing that the defect closely resembles $As_O$.

| Sample description | Atomic ratio % | | | | | |
|---|---|---|---|---|---|---|
| | Al 2p | Si 2p | C 1s | O 1s | Zn 2p1 | Zn 2p3 |
| Halloysite pure | 14.30 | 19.60 | 14.80 | 51.30 | | |
| ZnO seed-Halloysite | 16.30 | 18.00 | 12.90 | 51.30 | 1.40 | |
| ZnO-Halloysite | 1.60 | 40.60 | 21.00 | 23.10 | 7.80 | 5.90 |

**Table 8**. Surface atomic ratios of the samples from XPS analysis.

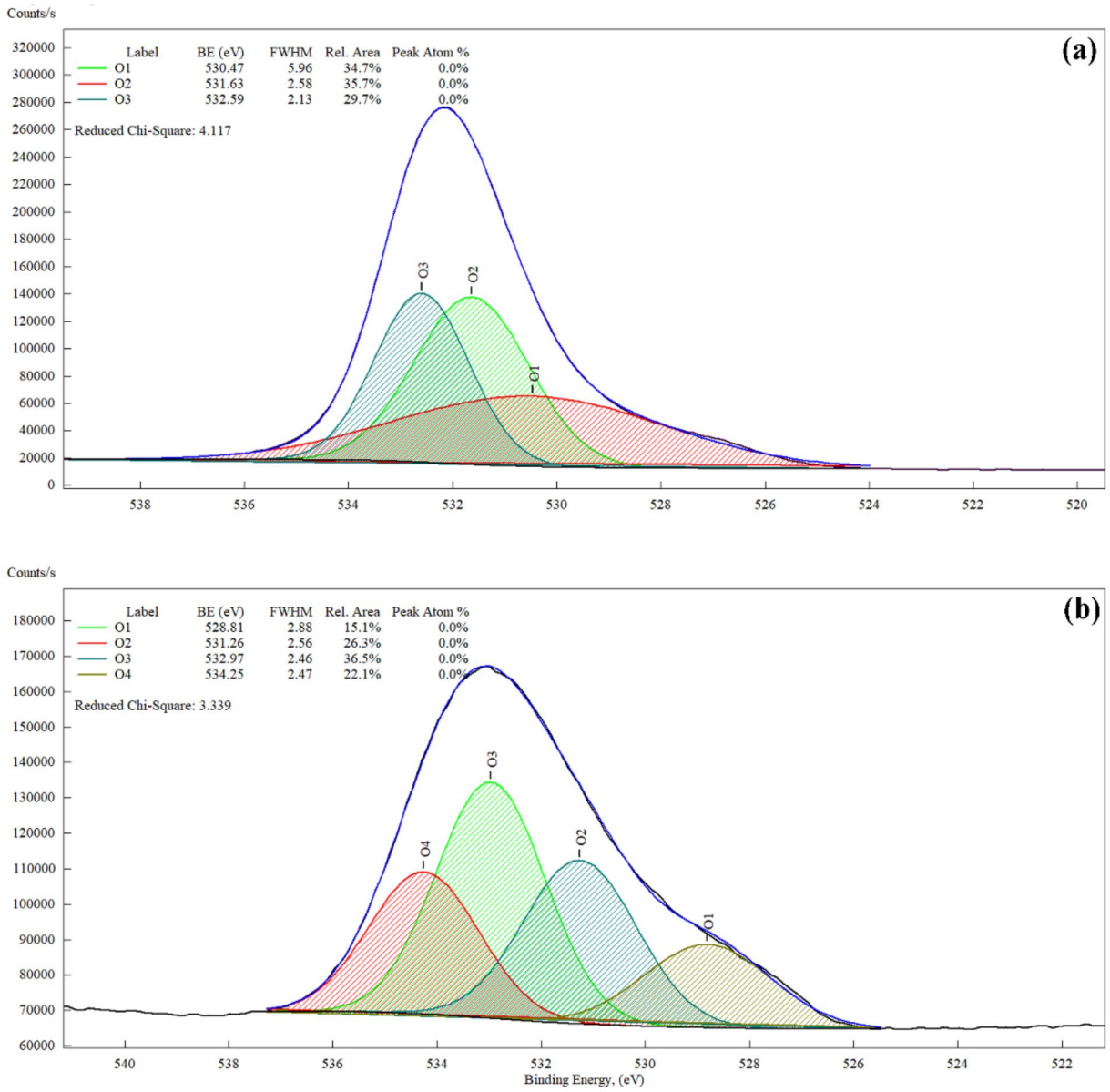


**Fig. 7**. O1s XPS spectrums for Halloysite pure (**a**) and ZnO-Halloysite (**b**).

## Conclusion

Box-Behnken Response Surface Design was used in this study to determine the optimal conditions for arsenic adsorption onto ZnO-Halloysite nanocomposite surface. According to the results, the adsorption conditions significantly affected the removal of arsenic. The interactive effect of five independent variables (initial arsenic concentration, pH, temperature, contact time, and adsorbent dose) on two responses (arsenic adsorption

| Adsorbent | Binding energy (eV) | Arsenic species | References |
|---|---|---|---|
| nZVI | 45.2<br>45<br>43.5 | As(V)<br>As(V)<br>As(III) | 79 |
| Ferromanganese slag | 43.75<br>44.90 | As(III)<br>As(V) | 80 |
| (Co–Al–Fe) nano adsorbent | 41.94<br>42.25<br>43.04<br>43.81<br>44.62<br>44.58 | As(III)<br>As(III)<br>As(III)<br>As(V)<br>As(V)<br>As(V) | 81 |
| $MnO_2$@$La(OH)_3$ Nanocomposite | 45.11<br>45.13<br>45.1<br>44.1 | As(V)<br>As(V)<br>As(V)<br>As(III) | 82 |

**Table 9**. As3d binding energy and arsenic species.

capacity and removal) was evaluated using response surface plots. A quadratic and linear mathematical model was developed based on statistical regression analysis of experimental data obtained from 43 batch runs for arsenic adsorption capacity and removal efficiency. At a 95% confidence level, the ANOVA results further established the significance ($P < 0.05$) of the quadratic model for arsenic adsorption capacity and the linear model for arsenic removal. By using the desirability function method, optimization of the adsorbent dosage (0.135 g), initial concentration (49.99 mg/L), temperature (25 °C), pH (3.99), and contact time (3.99 h) led to a maximum removal efficiency of 91.31% of arsenic with an adsorption capacity of 12.63 mg/g with 0.995 desirability. The arsenic adsorption mechanism onto ZnO-Halloysite was studied using FTIR and XPS analyses. Results indicated that maximum arsenic adsorption occurs between pH 7 and 8 due to As(III) adsorption during hard acid-hard base reactions or due to complexes formed between AS(III) and ZnO-Halloysite surface during AS(III) doping. Furthermore, arsenic adsorption in the form of As (VI) on ZnO-Halloysite was pronounced at high pH, which may be explained by the rapid oxidation of As(III) into As(VI) at high pHs.

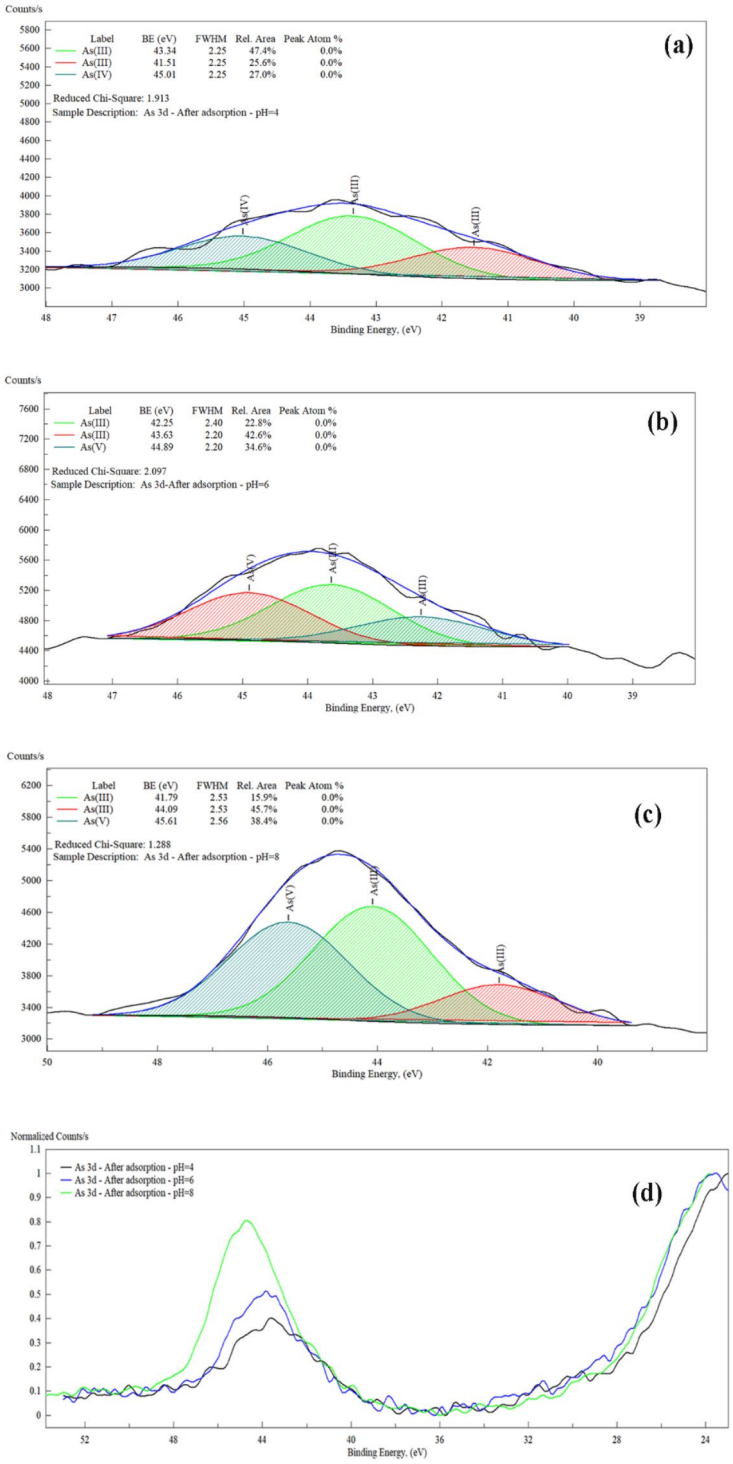


**Fig. 8**. As 3d spectrum in different pH: 4 (**a**), 6 (**b**), 8 (**c**) and Overlayer of As3d spectrum in different pH (**d**).

| pH range | ZnO-Halloysite after As (III) adsorption | | | | | | | | |
|---|---|---|---|---|---|---|---|---|---|
| | 4 | | | 6 | | | 8 | | |
| Binding energy | 41.51 | 43.34 | 45.01 | 42.25 | 43.63 | 44.89 | 41.79 | 44.09 | 45.61 |
| Atomic ratio % | 25.6 | 47.4 | 27 | 22.8 | 42.6 | 34.6 | 15.9 | 45.7 | 38.4 |
| Arsenic species | As(III) | As(III) | As(V) | As(III) | As(III) | As(V) | As(III) | As(III) | As(V) |

**Table 10**. Binding energy of As3d after adsorption as (III) upon ZnO-Halloysite.

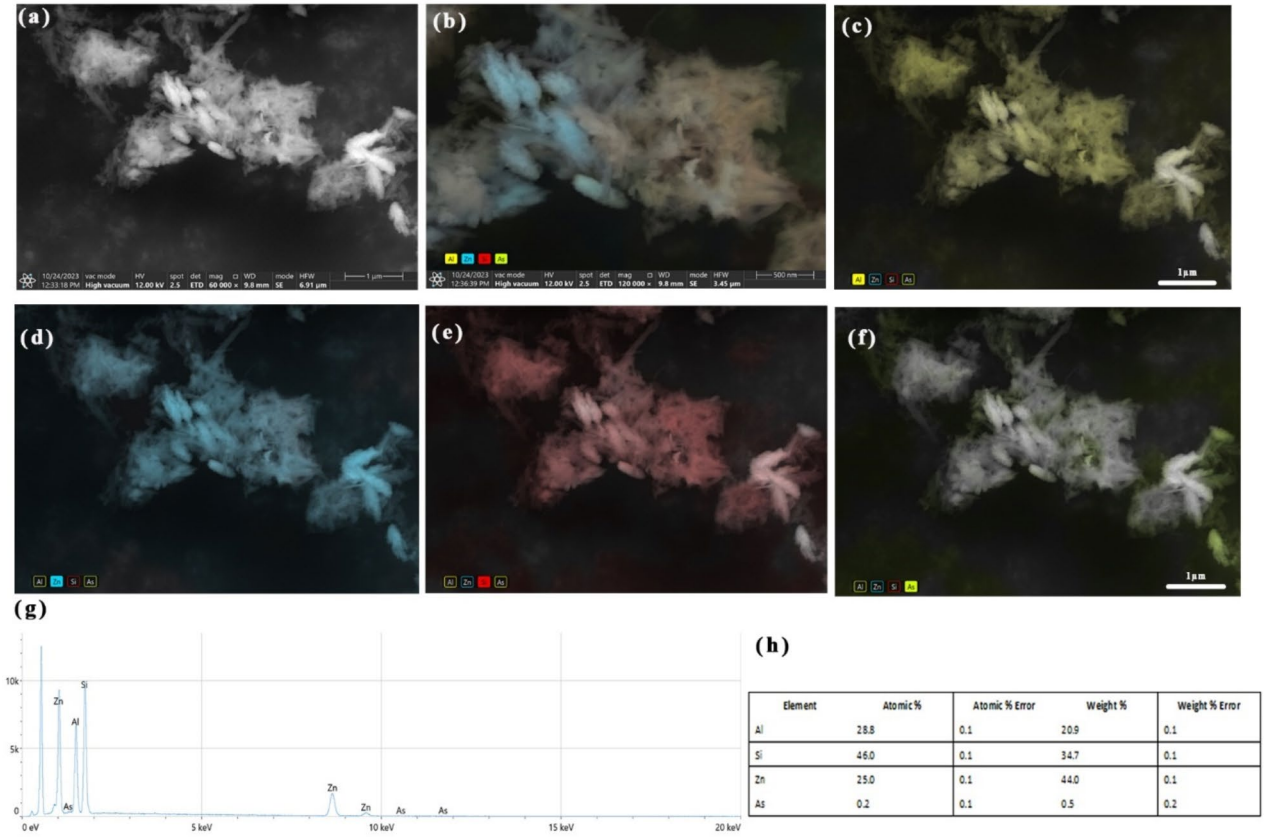


**Fig. 9**. Elemental mapping (**a**-**f**) and EDX spectrum (**g**-**h**) of ZnO-Halloysite nanocomposite after As(III) adsorption at pH = 8.

## Data availability

The data for this study will be available upon reasonable request by contacting the corresponding author (norouzbeigi@iust.ac.ir).

Received: 13 June 2024; Accepted: 11 September 2024
Published online: 16 September 2024

## References

1. Mohammed Abdul, K. S., Jayasinghe, S. S., Chandana, E. P. S., Jayasumana, C. & De Silva, P. M. C. S. Arsenic and human health effects: A review. *Environ. Toxic. Pharm.* **40**, 828–846. https://doi.org/10.1016/j.etap.2015.09.016 (2015).
2. Hamidian, A. H., Razeghi, N., Zhang, Y. & Yang, M. Spatial distribution of arsenic in groundwater of Iran, a review. *J. Geochemical Explor.* **201**, 88–98. https://doi.org/10.1016/j.gexplo.2019.03.014 (2019).
3. Patel, K. S. et al. A review on arsenic in the environment: contamination, mobility, sources, and exposure. *RSC Adv.* **13**, 8803–8821. https://doi.org/10.1039/D3RA00789H (2023).
4. Yu, J. et al. Simultaneous removal of arsenate and arsenite in water using a novel functional halloysite nanotube composite. *Environ. Sci. Pollut. Res.* **29**, 77131–77144. https://doi.org/10.1007/s11356-022-20261-7(2022) (2022).
5. Lou, S. et al. Enhanced removal of as(III) and as(V) from water by a novel zirconium-chitosan modified spherical sodium alginate composite. *Int. J. Biol. Macromol.* **176**, 304–314. https://doi.org/10.1016/j.ijbiomac.2021.02.077 (2021).
6. Garelick, H., Jones, H. & Dybowska, A. & Valsami-jones, E. Reviews of environmental contamination 197. *Nat. Hist.* **197**, (2008).

7. Goswami, A., Raul, P. K. & Purkait, M. K. Arsenic adsorption using copper (II) oxide nanoparticles. *Chem. Eng. Res. Des.* **90**, 1387–1396. https://doi.org/10.1016/j.cherd.2011.12.006 (2012).
8. Pasalari, H., Ghaffari, H. R., Mahvi, H., Pourshabanian, M. & Azari, A. Activated carbon derived from date stone as natural adsorbent for phenol removal from aqueous solution. *Desalin. Water Treat.* **72**, 406–417. https://doi.org/10.5004/dwt.2017.20686 (2017).
9. Cavallaro, G. et al. Organic-Nanoclay composite materials as removal agents for environmental decontamination. *RSC Adv.* **9**, 40553–40564. https://doi.org/10.1039/c9ra08230a (2019).
10. Wan Ikhsan, S. N., Yusof, N., Aziz, F. & Fauzi Ismail, A. Facile synthesis and characterization of Zno-HNT additive for enhancement of polysulfone membrane for Oil-in-water separation. *Mater. Today Proc.* **46**, 1978–1982. https://doi.org/10.1016/j.matpr.2021.02.589 (2021).
11. Joussein, E. et al. Halloysite clay minerals - a review. *Clay Min. - CLAY Min.* **40**, 383–426. https://doi.org/10.1180/0009855054040180 (2005).
12. Alharthi, S. S. Retention profile of as (III) and as (V) oxyanions from water onto polypyrrole. *J. King Saudi Univ. Sci.* **33**, 101285. https://doi.org/10.1016/j.jksus.2020.101285 (2021).
13. Weidner, E. & Ciesielczyk, F. Removal of hazardous oxyanions from the environment using metal-oxide-based materials. *Material (Basel)* **12**, 927. https://doi.org/10.3390/ma12060927 (2019).
14. Zhao, Y., Abdullayev, E., Vasiliev, A. & Lvov, Y. Halloysite nanotubule clay for efficient water purification. *J. Colloid Interface Sci.* **406**, 121–129. https://doi.org/10.1016/j.jcis.2013.05.072 (2013).
15. Ngulube, T., Gumbo, J. R., Masindi, V. & Maity, A. Evaluation of the efficacy of halloysite nanotubes in the removal of acidic and basic dyes from aqueous solution. *Clay Min.* **54**, 197–207. https://doi.org/10.1180/clm.2019.27 (2019).
16. Lun, H., Ouyang, J. & Yang, H. Enhancing dispersion of halloysite nanotubes via chemical modification. *Phys. Chem. Min.* **41**, 281–288. https://doi.org/10.1007/s00269-013-0646-9 (2014).
17. Filice, S. et al. Structural characterization and adsorption properties of dunino raw halloysite mineral for dye removal from water. *Materials* **14**, 3676. https://doi.org/10.3390/ma14133676 (2021).
18. Zhou, T., Li, C., Jin, H., Lian, Y. & Han, W. Effective Adsorption/Reduction of cr(VI) oxyanion by Halloysite@Polyaniline Hybrid nanotubes. *ACS Appl. Mater. Interfaces* **9**, 6030–6043. https://doi.org/10.1021/acsami.6b14079 (2017).
19. Mahmoudian, M. H. et al. Statistical modeling and optimization of dexamethasone adsorption from aqueous solution by Fe3O4@NH2-MIL88B nanorods: Isotherm, kinetics, and thermodynamic. *Environ. Res.* **236**, 116773. https://doi.org/10.1016/j.envres.2023.116773 (2023).
20. Kalantary, R. R. et al. Adsorption and magnetic separation of lead from synthetic wastewater using carbon/Iron oxide nanoparticles composite. *J. Maz Univ. Med. Sci.* **24**, 172–183 (2014).
21. Yang, W., Li, Q., Gao, S. & Shang, J. K. High efficient as(III) removal by self-assembled zinc oxide micro-tubes synthesized by a simple precipitation process. *J. Mater. Sci.* https://doi.org/10.1007/s10853-011-5542-4 (2011).
22. Khoddam, M. A., Norouzbeigi, R., Velayi, E. & Cavallaro, G. Facile synthesis of ZnO/Hal nanocomposite for arsenite (as(III)) removal from aqueous media. *Sci. Rep.* **131 13**, 1–20. https://doi.org/10.1038/s41598-023-48531-5 (2023).
23. Mudzielwana, R., Gitari, M. W. & Ndungu, P. Enhanced as(III) and as(V) adsorption from aqueous solution by a clay based hybrid sorbent. *Front. Chem.* https://doi.org/10.3389/fchem.2019.00913 (2020).
24. Mutar, R. F. & Saleh, M. A. Optimization of arsenic ions adsorption and removal from hospitals wastewater by nano-bentonite using central composite design. *Mater. Today Proc.* **60**, 1248–1256. https://doi.org/10.1016/j.matpr.2021.08.213 (2022).
25. Mendoza-Chávez, C. E. et al. Statistical optimization of arsenic removal from synthetic water by electrocoagulation system and its application with real arsenic-polluted groundwater. *Environ. Technol.* **42**, 3463–3474. https://doi.org/10.1080/09593330.2020.1732472 (2021).
26. Ehsani, A. et al. Towards model-based optimization for quality by design in biotherapeutics production. *Comput. Aided Chem. Eng.* **46**, 25–30. https://doi.org/10.1016/B978-0-12-818634-3.50005-9 (2019).
27. Maity, S. Applications of selected response surface design of experiments and advanced control charts in textile engineering. *Text. Calc Fibre Finish. Garment.* **13-55** https://doi.org/10.1016/B978-0-323-99041-7.00015-1 (2023).
28. Adlnasab, L., Shekari, N. & Maghsodi, A. Optimization of arsenic removal with Fe3O4@Al2O3@Zn-Fe LDH as a new magnetic nano adsorbent using Box-Behnken design. *J. Environ. Chem. Eng.* **7**, 102974. https://doi.org/10.1016/j.jece.2019.102974 (2019).
29. Hashemi, S. Y., Azari, A., Raeesi, M. & Yaghmaeian, K. Application of response surface methodology (RSM) in optimisation of fluoride removal by magnetic chitosan/graphene oxide composite: kinetics and isotherm study. *Int. J. Environ. Anal. Chem.* **103**, 5368–5386. https://doi.org/10.1080/03067319.2021.1938021 (2023).
30. Azari, A. et al. Which is better for optimizing the biosorption process of lead – central composite design or the Taguchi technique? *Water Sci. Technol.* **74**, 1446–1456. https://doi.org/10.2166/wst.2016.318 (2016).
31. Li, J. et al. Arsenate removal from water by Ti electrocoagulation: Main influencing factors, response surface optimization, and potential mechanisms. *J. Water Process. Eng.* **54**, 104042. https://doi.org/10.1016/j.jwpe.2023.104042f (2023).
32. Bayuo, J., Rwiza, M. J. & Mtei, K. M. Modeling and optimization of trivalent arsenic removal from wastewater using activated carbon produced from maize plant biomass: A multivariate experimental design approach. *Biomass Convers. Biorefinery.* 1–24. https://doi.org/10.1007/S13399-023-04494-1/METRICS (2023).
33. Okolo, B. I. et al. Adsorption of lead(II) from aqueous solution using Africa Elemi seed, mucuna shell and oyster shell as adsorbents and optimization using box–behnken design. *Appl. Water Sci.* **10**, 1–23. https://doi.org/10.1007/s13201-020-01242-y (2020).
34. Kobya, M., Demirbas, E., Gebologlu, U., Oncel, M. S. & Yildirim, Y. Optimization of arsenic removal from drinking water by electrocoagulation batch process using response surface methodology. *Desalin. Water Treat.* **51**, 6676–6687 (2013).
35. Song, J., Jia, S. Y., Ren, H. T., Wu, S. H. & Han, X. Application of a high-surface-area schwertmannite in the removal of arsenate and arsenite. *Int. J. Environ. Sci. Technol.* **12**, 1559–1568. https://doi.org/10.1007/s13762-014-0528-9 (2015).
36. Nikosokhan, R., Norouzbeigi, R. & Velayi, E. Fabrication of cobalt-based superhydrophobic coating with micro/nano hierarchical structure without additional hydrophobization treatment. *Ceram. Int.* **47**, 30711–30721. https://doi.org/10.1016/j.ceramint.2021.07.250 (2021).
37. Han, C. et al. The optimization of as(V) removal over mesoporous alumina by using response surface methodology and adsorption mechanism. *J. Hazard. Mater.* **254–255**, 301–309. https://doi.org/10.1016/j.jhazmat.2013.04.008 (2013).
38. Watson, M. A. et al. Response surface methodology investigation into the interactions between arsenic and humic acid in water during the coagulation process. *J. Hazard. Mater.* **312**, 150–158. https://doi.org/10.1016/j.jhazmat.2016.03.002 (2016).
39. Zare Pirhaji, J., Moeinpour, F., Mirhoseini Dehabadi, A. & Yasini Ardakani, S. A. Synthesis and characterization of halloysite/graphene quantum dots magnetic nanocomposite as a new adsorbent for pb(II) removal from water. *J. Mol. Liq.* **300**, 112345. https://doi.org/10.1016/j.molliq.2019.112345 (2020).
40. Talib, N. A. A., Salam, F., Yusof, N. A., Alang Ahmad, S. A. & Sulaiman, Y. Modeling and optimization of electrode modified with poly(3,4-ethylenedioxythiophene)/graphene oxide composite by response surface methodology/Box-Behnken design approach. *J. Electroanal. Chem.* **787**, 1–10. https://doi.org/10.1016/j.jelechem.2017.01.032 (2017).
41. Taheri, M. Techno-economical aspects of electrocoagulation optimization in three acid azo dyes' removal comparison. *Clean. Chem. Eng.* **2**, 100007. https://doi.org/10.1016/j.clce.2022.100007 (2022).
42. Rahman, N. & Ahmad, I. Insights into the statistical physics modeling and fractal like kinetic approach for the adsorption of as(III) on coordination polymer gel based on zirconium(IV) and 2-thiobarbituric acid. *J. Hazard. Mater.* **457**, 131783. https://doi.org/10.1016/j.jhazmat.2023.131783 (2023).

43. Alam, P. et al. Box-Behnken Design (BBD) application for optimization of chromatographic conditions in RP-HPLC method development for the estimation of thymoquinone in nigella sativa seed powder. *Process* **10**, 1082. https://doi.org/10.3390/pr10061082 (2022).
44. Azari, A. et al. Magnetic NH2-MIL-101(Al)/Chitosan nanocomposite as a novel adsorbent for the removal of azithromycin: Modeling and process optimization. *Sci. Rep.* **121**(12), 1–16. https://doi.org/10.1038/s41598-022-21551-3 (2022).
45. Ray, S. & Lalman, J. A. Using the box–benkhen design (BBD) to minimize the diameter of electrospun titanium dioxide nanofibers. *Chem. Eng. J.* **169**, 116–125. https://doi.org/10.1016/j.cej.2011.02.061 (2011).
46. Kumari, M. & Gupta, S. K. Response surface methodological (RSM) approach for optimizing the removal of trihalomethanes (THMs) and its precursor's by surfactant modified magnetic nanoadsorbents (sMNP) - an endeavor to diminish probable cancer risk. *Sci. Rep.* **91**(9), 1–11. https://doi.org/10.1038/s41598-019-54902-8 (2019).
47. Yuan, S. & Chen, H. Mathematical rules for synergistic, additive, and antagonistic effects of multi-drug combinations and their application in research and development of combinatorial drugs and special medical food combinations. *Food Sci. Hum. Wellness* **8**, 136–141. https://doi.org/10.1016/j.fshw.2019.01.003 (2019).
48. Elagouz, A. et al. Utilization of response surface method (RSM) in optimizing automotive air conditioning (AAC) performance exerting Al2O3/PAG Nanolubricant. *J. Phys. Conf. Ser.* **1532** https://doi.org/10.1088/1742-6596/1532/1/012003 (2020).
49. Wei, Z. et al. The effect of pH on the adsorption of arsenic(III) and arsenic(V) at the TiO2 anatase [101] surface. *J. Colloid Interface Sci.* **462**, 252–259. https://doi.org/10.1016/j.jcis.2015.10.018 (2016).
50. Alshgari, R. A. et al. ZnO Nanostructures doped with various chloride ion concentrations for efficient photocatalytic degradation of methylene blue in alkaline and acidic media. *Molecules* **27**, 8726. https://doi.org/10.3390/molecules27248726 (2022).
51. Faroudi, L. et al. Facile and sustainable synthesis of ZnO nanoparticles: Effect of gelling agents on ZnO shapes and their photocatalytic performance. *ACS Omega* https://doi.org/10.1021/ACSOMEGA.3C01491 (2023).
52. Degen, A. & Kosec, M. Effect of pH and impurities on the surface charge of zinc oxide in aqueous solution. *J. Eur. Ceram. Soc.* **20**, 667–673. https://doi.org/10.1016/S0955-2219(99)00203-4 (2000).
53. Li, H. X., Wang, Y. & Cang, D. Q. Zinc leaching from electric arc furnace dust in alkaline medium. *J. Cent. South. Univ. Technol. (English Ed.)* **17**, 967–971. https://doi.org/10.1007/s11771-010-0585-2 (2010).
54. Wang, X. et al. Roles of pH, cation valence, and ionic strength in the stability and aggregation behavior of zinc oxide nanoparticles. *J. Environ. Manag.* **267**, 110656. https://doi.org/10.1016/j.jenvman.2020.110656 (2020).
55. Krężel, A. & Maret, W. The biological inorganic chemistry of zinc ions. *Arch. Biochem. Biophys.* **611**, 3–19. https://doi.org/10.1016/j.abb.2016.04.010 (2016).
56. Bera, S., Dhara, S., Velmurugan, S. & Tyagi, A. K. Analysis on binding energy and auger parameter for estimating size and stoichiometry of ZnO nanorods. *Int. J. Spectrosc.* 1–4, (2012). https://doi.org/10.1155/2012/371092 (2012).
57. Al-Gaashani, R., Zakaria, Y., Gladich, I., Kochkodan, V. & Lawler, J. XPS, structural and antimicrobial studies of novel functionalized halloysite nanotubes. *Sci. Rep.* **12**, 21633. https://doi.org/10.1038/s41598-022-25270-7 (2022).
58. Kubala-Kukuś, A. et al. X-ray photoelectron spectroscopy analysis of chemically modified halloysite. *Radiat. Phys. Chem.* **175**, 108149. https://doi.org/10.1016/j.radphyschem.2019.02.008 (2020).
59. Kumar, V. et al. The role of growth atmosphere on the structural and optical quality of defect free ZnO films for strong ultraviolet emission. *Laser Phys.* **24** https://doi.org/10.1088/1054-660X/24/10/105704 (2014).
60. Wang, H., Wu, D., Li, X. & Huo, P. Ce doping TiO2/halloysite nanotubes photocatalyst for enhanced electrons transfer and photocatalytic degradation of tetracycline. *J. Mater. Sci. Mater. Electron.* **30**, 19126–19136. https://doi.org/10.1007/s10854-019-02268-y (2019).
61. Vishnuraj, R., Karuppanan, K. K., Aleem, M. & Pullithadathil, B. Boosting the performance of NO2 gas sensors based on n–n type mesoporous ZnO@In2O3 heterojunction nanowires: In situ conducting probe atomic force microscopic elucidation of room temperature local electron transport. *Nanoscale Adv.* **2**, 4785–4797. https://doi.org/10.1039/D0NA00318B (2020).
62. Feng, W. et al. Wet chemistry synthesis of ZnO crystals with hexamethylenetetramine(HMTA): Understanding the role of HMTA in the formation of ZnO crystals. *Mater. Sci. Semicond. Process.* **41**, 462–469. https://doi.org/10.1016/j.mssp.2015.10.017 (2016).
63. Althumairi, N. A. et al. Structural, morphological, optical, and electrical studies of Tb-doped ZnO micropods elaborated by chemical bath deposition on a p-Si substrate. *Appl. Phys. Mater. Sci. Process.* **128** https://doi.org/10.1007/s00339-022-05701-y (2022).
64. Barrera-Andrade, J. M. et al. In situ formation of CuxO/ZnO photocatalysts for efficient simultaneous oxidation of as (III) and adsorption of as (V): Effect of Cu loading. *Environ. Sci. Pollut Res.* https://doi.org/10.1007/s11356-023-31480-x (2023).
65. Marrani, A. G., Caprioli, F., Boccia, A., Zanoni, R. & Decker, F. Electrochemically deposited ZnO films: An XPS study on the evolution of their surface hydroxide and defect composition upon thermal annealing. *J. Solid State Electrochem.* **18**, 505–513. https://doi.org/10.1007/s10008-013-2281-2 (2014).
66. Li, Y. et al. Micro/Nano hierarchical peony-like Al doped ZnO superhydrophobic film: The guiding effect of (100) preferred seed layer. *Sci. Rep.* **6**, 19187. https://doi.org/10.1038/srep19187 (2016).
67. Long, X. et al. Heterojunction and oxygen vacancy modification of ZnO nanorod array photoanode for enhanced photoelectrochemical water splitting. *ChemSusChem* **11**, 4094–4101. https://doi.org/10.1002/cssc.201801828 (2018).
68. Lei, J., Liu, W., Jin, Y. & Li, B. Oxygen vacancy-dependent chemiluminescence: A facile approach for quantifying oxygen defects in ZnO. *Anal. Chem.* **94**, 8642–8650. https://doi.org/10.1021/acs.analchem.2c00359 (2022).
69. Lim, S. F., Zheng, Y. M. & Chen, J. P. Organic arsenic adsorption onto a magnetic sorbent. *Langmuir* **25**, 4973–4978. https://doi.org/10.1021/la802974x (2009).
70. Ren, X. et al. Adsorption of arsenic on modified montmorillonite. *Appl. Clay Sci.* 97–98. https://doi.org/10.1016/j.clay.2014.05.028 (2014).
71. Xiao, K., Zhang, Y., Gong, Y. & Zhang, Y. Preparation of zinc oxide/halloysite compound and their reinforcement for styrene butadiene rubber composite. *Appl. Clay Sci.* **243**, 107078. https://doi.org/10.1016/j.clay.2023.107078 (2023).
72. Kim, B. H. & Kwon, J. W. Metal catalyst for low-temperature growth of controlled zinc oxide nanowires on arbitrary substrates. *Sci. Rep.* **4**, 4379. https://doi.org/10.1038/srep04379 (2014).
73. Kwoka, M., Kulis-Kapuscinska, A., Zappa, D., Comini, E. & Szuber, J. Novel insight on the local surface properties of ZnO nanowires. *Nanotechnology* **31** https://doi.org/10.1088/1361-6528/ab8dec (2020).
74. Privezentsev, V. V., Tabachkova, N. Y. & Lebedinskii, Y. Y. HRTEM and XPS study of nanoparticle formation in zn + ion implanted Si. *AIP Conf. Proc.* **1583**, 109–113. https://doi.org/10.1063/1.4865615 (2014).
75. Reddy, K. J., McDonald, K. J. & King, H. A novel arsenic removal process for water using cupric oxide nanoparticles. *J. Colloid Interface Sci.* **397**, 96–102. https://doi.org/10.1016/j.jcis.2013.01.041 (2013).
76. Martinson, C. A. & Reddy, K. J. Adsorption of arsenic(III) and arsenic(V) by cupric oxide nanoparticles. *J. Colloid Interface Sci.* **336**, 406–411. https://doi.org/10.1016/j.jcis.2009.04.075 (2009).
77. Antonatos, N., Luxa, J., Sturala, J. & Sofer, Z. Black arsenic: A new synthetic method by catalytic crystallization of arsenic glass. *Nanoscale* **12**, 5397–5401. https://doi.org/10.1039/C9NR09627B (2020).
78. Han, X. et al. As(III) removal and speciation of Fe (Oxyhydr)oxides during simultaneous oxidation of as(III) and Fe(II). *Chemosphere* **147**, 337–344. https://doi.org/10.1016/j.chemosphere.2015.12.128 (2016).
79. Horzum, N., Demir, M. M., Nairat, M. & Shahwan, T. Chitosan fiber-supported zero-valent iron nanoparticles as a novel sorbent for sequestration of inorganic arsenic. *RSC Adv.* **3**, 7828–7837. https://doi.org/10.1039/c3ra23454a (2013).

80. Jain, N. & Maiti, A. Arsenic adsorbent derived from the ferromanganese slag. *Environ. Sci. Pollut. Res.* **28**, 3230–3242. https://doi.org/10.1007/s11356-020-10745-9 (2021).
81. Penke, Y. K., Anantharaman, G., Ramkumar, J. & Kar, K. K. Aluminum substituted cobalt ferrite (Co-Al-Fe) nano adsorbent for arsenic adsorption in aqueous systems and detailed redox behavior study with XPS. *ACS Appl. Mater. Interfaces* **9**, 11587–11598. https://doi.org/10.1021/acsami.6b16414 (2017).
82. Wang, Y. et al. Arsenic oxidation and removal from water via Core–Shell MnO2@La(OH)3 nanocomposite adsorption. *Int. J. Environ. Res. Public Health* **19**, 10649. https://doi.org/10.3390/ijerph191710649 (2022).
83. Mohamed, C. H. I. B. A. N. Application of low-cost adsorbents for arsenic removal: A review. *J. Environ. Chem. Ecotoxicol.* **4** https://doi.org/10.5897/JECE11.013 (2012).
84. Uppal, H., Hemlata, Tawale, J. & Singh, N. Zinc peroxide functionalized synthetic graphite: An economical and efficient adsorbent for adsorption of arsenic (III) and (V). *J. Environ. Chem. Eng.* **4**, 2964–2975. https://doi.org/10.1016/j.jece.2016.05.038 (2016).
85. Chen, Y. J. et al. The study of rapid thermal annealing on arsenic-doped ZnO for the p-type ZnO formation. *J. Cryst. Growth* **362**, 193–196. https://doi.org/10.1016/j.jcrysgro.2012.03.060 (2013).
86. Limpijumnong, S., Zhang, S. B., Wei, S. H. & Park, C. H. Doping by large-size-mismatched impurities: the microscopic origin of arsenic- or antimony-doped p-type zinc oxide. *Phys. Rev. Lett.* **92** https://doi.org/10.1103/PhysRevLett.92.155504 (2004).
87. Puchala, B. & Morgan, D. Stable interstitial dopant-vacancy complexes in ZnO. *Phys. Rev. B -Condens. Matter Mater. Phys.* **85**, 195207. https://doi.org/10.1103/PhysRevB.85.195207 (2012).
88. Guan, H. et al. Study of arsenic doping ZnO thin films grown by metal–organic chemical vapor depositionvia x-ray photoelectron spectroscopy. *J. Phys. Condens. Matter* **20** https://doi.org/10.1088/0953-8984/20/29/292202 (2008).
89. Snigurenko, D. et al. XPS study of arsenic doped ZnO grown by atomic layer deposition. *J. Alloys Compd.* **582**, 594–597. https://doi.org/10.1016/j.jallcom.2013.08.061 (2014).
90. Weng, L. W. et al. Characterizations of arsenic-doped zinc oxide films produced by atmospheric metal-organic chemical vapor deposition. *Appl. Surf. Sci.* **277**, 1–6. https://doi.org/10.1016/j.apsusc.2013.03.005 (2013).
91. Xu, N. et al. Arsenic doping for synthesis of nanocrystalline p-type ZnO thin films. *J. Vac. Sci. Technol. A* **24**, 517–520. https://doi.org/10.1116/1.2194939 (2006).
92. Biswas, P., Nath, P., Sanyal, D. & Banerji, P. An alternative approach to investigate the origin of p-type conductivity in arsenic doped ZnO. *Curr. Appl. Phys.* **15**, 1256–1261. https://doi.org/10.1016/j.cap.2015.07.015 (2015).
93. Fan, J. C. et al. Arsenic doped p -type zinc oxide films grown by radio frequency magnetron sputtering. *J. Appl. Phys.* **106** https://doi.org/10.1016/j.apsusc.2019.144273 (2009).


## Author contributions

M.A.K.: Writing—Original Draft, Methodology, Investigation, software, Formal analysis. R.N.: Supervision, Conceptualization, Resources. E.V.: Writing—Review & Editing, Supervision, Conceptualization, Methodology. G.C.: Supervision, software, Methodology.

## Declarations

## Competing interests

The authors declare no competing interests.

## Additional information

**Correspondence** and requests for materials should be addressed to R.N.

**Reprints and permissions information** is available at www.nature.com/reprints.

**Publisher's note** Springer Nature remains neutral with regard to jurisdictional claims in published maps and institutional affiliations.